

Article

Transferrin-Grafted Albumin Nanoparticles for the Targeted Delivery of Apocynin and Neuroprotection in an In Vitro Model of the BBB

Venkatesan Perumal ^{1,*}, Arun Reddy Ravula ¹, Agnieszka Agas ¹, Manisha Kannan ¹, Xiangshan Liu ² , Shanmuga Sundari I ³, Sivakumar Vijayaraghavalu ⁴, James Haorah ¹, Yuanwei Zhang ² and Namas Chandra ^{1,*}

¹ Center for Injury Biomechanics, Materials, and Medicine, Department of Biomedical Engineering, New Jersey Institute of Technology, Newark, NJ 07102, USA

² Department of Chemistry and Environmental Science, New Jersey Institute of Technology, Newark, NJ 07102, USA

³ Computational Biology Special Lab, Department of Biotechnology, Bannari Amman Institute of Technology, Sathyamangalam 638401, India

⁴ Department of Life Sciences (Zoology), Manipur University, Imphal 795003, India

* Correspondence: perumal@njit.edu or venbio55@gmail.com (V.P.); namas.chandra@njit.edu (N.C.)

Abstract: Traumatic brain injury (TBI) is a major cause of morbidity and mortality worldwide, affecting over 10 million people annually, with an estimated cost of \$76.5 billion. Although apocynin freely transverse the blood–brain barrier (BBB), its application is limited due to its rapid elimination, low terminal half-life ($t_{1/2} = 6.7$ min), narrow dose–response relationship, and cytotoxicity, thereby requiring repeated dosages. With this study, we aimed to develop transferrin-functionalized nanoparticles encapsulating apocynin to treat neuroinflammation for targeted drug delivery to sites of brain injury. As a preliminary approach, we endeavored to optimize the formulation parameters of apocynin-loaded albumin nanoparticles prepared through the desolvation method. The nanoparticles were characterized for their size, polydispersity, surface charge, drug loading and in vitro drug release. In this study, we also investigated the anti-inflammatory and neuroprotective effects of free apocynin and nanoparticle-loaded apocynin in neuronal cells. We show that the developed formulation displayed monodispersed, nanosized particles with higher entrapment efficiency, loading, stability, and sustained release profiles. The permeability of the nanoparticles across HBMECs reached the maximum at 67%. The in vivo evaluation revealed the enhanced uptake of transferrin-anchored nanoparticles in the brain tissues when compared with unmodified nanoparticles after I.V. administration. In vivo nanoparticle localization studies using a blast TBI (bTBI) model and confocal fluorescence microscopy have shown that tf-apoANPs are successful in delivering relatively high amounts of nanoparticles to the brain parenchyma and glial cells compared to non-targeted nanoparticles. We also establish that targeted nanoparticles accumulate in the brain. In conclusion, tf-apoANPs are efficacious carriers for targeted delivery across the blood–brain barrier to potentially treat neuroinflammation in brain injury and other diseases.

Keywords: apocynin; nanoparticle; albumin; HPLC; desolvation method; targeted delivery; biodistribution; neuroprotection



Citation: Perumal, V.; Ravula, A.R.; Agas, A.; Kannan, M.; Liu, X.; I, S.S.; Vijayaraghavalu, S.; Haorah, J.; Zhang, Y.; Chandra, N. Transferrin-Grafted Albumin Nanoparticles for the Targeted Delivery of Apocynin and Neuroprotection in an In Vitro Model of the BBB. *Micro* **2023**, *3*, 84–106. <https://doi.org/10.3390/micro3010008>

Academic Editors: Xi Yao, Yung-Fu Chang and Ming-Liang He

Received: 20 December 2022

Revised: 9 January 2023

Accepted: 11 January 2023

Published: 23 January 2023



Copyright: © 2023 by the authors. Licensee MDPI, Basel, Switzerland. This article is an open access article distributed under the terms and conditions of the Creative Commons Attribution (CC BY) license (<https://creativecommons.org/licenses/by/4.0/>).

1. Introduction

A traumatic brain injury (TBI) is a sudden injury from an external force that is associated with long-term cognitive deficits relating to trauma-induced neurodegeneration [1,2]. The preclinical research indicates that TBI is caused by secondary injury mechanisms (oxidative stress, neuroinflammation, and neurodegeneration) that severely affect the quality of life of military personnel returning from combat zones [2,3]. Previous studies from our laboratory established that under mild TBI conditions, the generation of free-radical-generating

enzymes, the expression of oxidative damage markers, BBB leakage, and neuroinflammation occur [4]. The published results show that the degradation of the tight junction (TJ) proteins and perivascular units by MMPs (matrix metalloproteinases) promotes BBB leakiness, vascular fluid cavitation, edema formation, and neuroinflammation. In a separate study, we also showed that animals exposed to moderate blast injury experienced increased oxidative stress due to the activation of microglial cells and subsequent activation of the superoxide-producing enzyme NADPH (nicotinamide adenine dinucleotide phosphate) oxidase (NOX) and neuroinflammation [4]. These factors synergistically enhanced the BBB damage several hours after the blast. Collectively, these studies confirm that primary-blast TBI induces the upregulation of NADPH oxidase isoforms in different regions of the brain parenchyma and that neurons appear to be at higher risk for oxidative damage compared with other neural cells. Hence, NOX-mediated oxidative stress is a potential target for the treatment of neuroinflammation, brain injury, and neurological dysfunction using a naturally occurring NADPH oxidase inhibitor called apocynin [5–7]. It completely blocks the increase in superoxide levels in different brain regions following a blast.

Apocynin (APO) (Figure 1) is a bioactive phytochemical derived from the roots of *Apocynum cannabinum* (Canadian hemp) or *Picrorhiza kurroa*, both of which are indigenous to the Himalayas. APO has an NOX-inhibitory effect and is an effective nicotinamide adenine dinucleotide (NADH) oxidase complex inhibitor that is extensively used in both traditional and modern-day therapeutic strategies to combat neuronal disorders [8,9]. Apocynin has anti-inflammatory and antioxidant effects as a result of its well-known mechanism, which involves the particular inhibition of nicotinamide adenine dinucleotide phosphate (NADPH) oxidase, as well as the suppression of a number of pro-inflammatory mediators [8]. Further, a previous study showed that the intraperitoneal administration of apocynin specifically inhibits the assembly of NOX subunits (by inhibiting the translocation of the p47phox subunit from cytosol to plasma membranes) and prevented secondary BBB damage in a rat model (4 h post-blast) by restoring the dislodged tight junction proteins from the endothelial capillaries [10]. However, its therapeutic efficacy is limited by its lower solubility and bioavailability; thus, a suitable nanocarrier system to overcome such limitations is needed [11]. Drug delivery to the brain is becoming more and more important but is severely restricted by the blood–brain barrier, which severely restricts the therapy of many neurological diseases [12]. Most small molecular drugs are rapidly eliminated via hepatic metabolism and renal excretion, and because of the short half-life in the circulation and reduced drug diffusion through the blood–brain barrier (BBB), only a limited fraction of the drug reaches the brain target site due to reduced drug diffusion through the blood–brain barrier (BBB) [13,14]. Similarly, the anti-neuroinflammatory drug, apocynin, also demonstrated minimal clinical impact due to its pharmaceutical impediments, such as its low aqueous solubility, poor oral bioavailability (<10%), rapid elimination (half-life $t_{1/2} = 6.7$ min), high protein binding rate, and narrow dose–response relationship [15]. Further, studies have revealed that mice treated with apocynin at 3.75 mg/kg (22%) showed a comparable mortality rate to vehicle-treated mice, although apocynin-treated mice (5.0 mg/kg) tended to have a higher mortality rate (38%) [16]. Hence the blood–brain barrier (BBB) represents a considerable obstacle to the brain entry of the majority of drugs to show therapeutic effects [17].

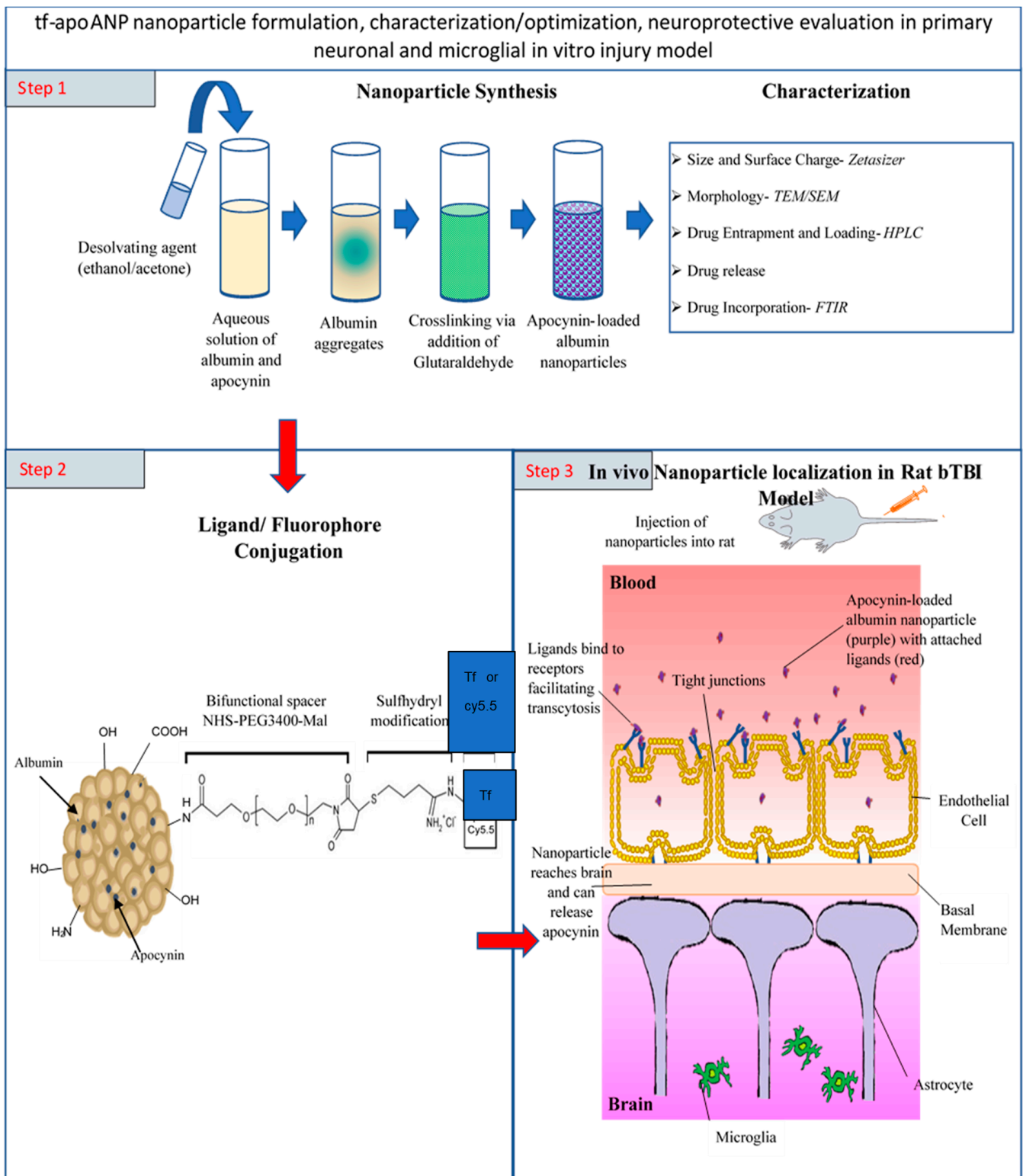


Figure 1. A schematic illustration of apocynin-loaded, TfR-targeted albumin nanoparticle (tf-apoANP) synthesis using the cross-linking method and characterization. Covalent conjugation of transferrin and FITC to BSA nanoparticles. Ligand-conjugated apoANPs can enter the CNS through the impaired BBB and BBB endothelium via receptor-mediated transcytosis.

Nanoparticles have previously been shown to permit the transport of a number of drugs across the BBB that normally cannot cross this barrier after intravenous injection [12].

The first nanoparticle system that was shown to transport molecules across the blood–brain barrier was polysorbate 80-coated poly(butyl cyanoacrylate) nanoparticles [12]. Nanoparticles coated with polysorbates have previously been shown to enable the transport of several drugs across the blood–brain barrier, which under normal circumstances is impermeable to these compounds [12]. Kreuter et al., (2002) postulated that the polysorbate coating led to the adsorption of apolipoprotein E and possibly apolipoprotein B from the blood after the I.V. injection. Thus, the nanoparticles could mimic lipoprotein particles, which would then interact with the lipoprotein receptors located on the brain capillary endothelial cells. A subsequent endocytosis of the nanoparticles together with bound drugs would then occur [12]. Similarly, transferrin (Tf), a hydrophilic transport vector, controls the extracellular iron level in the body fluid via binding and sequestration [18]. Tf receptors are over-expressed BBB endothelial cells [18] and are widely studied (for instance, R17217 and OX26 monoclonal antibodies) for endocytosis-mediated cellular uptake for the drug delivery of anticancer drugs [19–22]. Since the transferrin receptor is also present in the blood–brain barrier, transferrin-conjugated solid lipid nanoparticles enabled the enhanced delivery of quinine dihydrochloride to the brain [18]. The main structure of Tf is a b-1 glycoprotein comprising a single polypeptide chain of 698 amino acids with a molecular weight of 78 kDa. Serum Tf, ovotransferrin, lactoferrin, and melanotransferrin are the four typical types of naturally occurring Tfs. Chemically differentiated microdomains on the endothelial membrane express Tf receptors (TfRs), which are homodimeric glycoproteins with a molecular weight of 180 kDa. In a study on the regional distribution of TfR, a high density of TfR was observed in the neocortex of the human brain. In addition, a localized TfR in clathrin-coated vesicles can incorporate up to four Tf molecules and activated receptor-mediated transcytosis across the luminal membrane of brain microvascular endothelial cells (BMECs). TfR has also been targeted to improve the BBB passage by numerous researchers [18]. Tf-conjugated liposomes, poly(lactic acid), and PEGylated polycyanoacrylate can induce a high affinity to the brain. Paclitaxel-loaded particles coupled with Tf ligands can promote an antiproliferative effect on the growth of breast tumoral cells [18].

Albumin nano- and microspheres have been extensively exploited as carriers for drug targeting. Albumin serves as carrier matrix as it is biodegradable in nature. Albumin nanoparticles, besides being biodegradable, are relatively easy to process, and by varying the preparation conditions their size range and surface characteristics can be modified and controlled [20]. They are relatively non-toxic and non-immunogenic and produce no short-term adverse immunological consequences with serial injections. Currently, the mechanism of drug delivery to the brain lacks the ability to maintain sufficient drug concentrations at the target site and release the entrapped drug in a sustained manner for longer periods [21]. Hence, a novel nanocarrier possessing a particle diameter <200 nm, non-toxicity, prolonged circulation times, biodegradability, a sustained release profile, and biocompatibility would be considered a good candidate for drug delivery across the BBB [22,23].

Taken together, nanoparticles formulated with albumin offer the advantages of non-immunogenicity (endogenous protein 35–50 g/L human serum), biocompatibility, and excellent lyoprotection as a shelf-stable nanomedicine. Further, albumin presents a long half-life (19 days) that increases the plasma area under the curve (AUC) value, thereby maintaining a high blood drug concentration for a relatively long time. Hence, a novel albumin nanoparticle covalently coupled with a ligand (transferrin) offers the advantage of delivering drug molecules across the BBB through receptor-mediated uptake by brain capillary endothelial cells and localization at the parenchymal injury site in the brain (Figure 1). Hence, our present investigation comprises the development of transferrin-anchored pegylated albumin nanoparticles (Tf-PEG-NPs) as novel carriers for drug localization in brain tissues. We use a bifunctional PEG, maleimide–polyethyleneglycol–N-hydroxy succinimide (maleimide-PEG-NHS), containing a maleimide group at one terminus and a N-hydroxy succinimide at the other, to prepare a maleimide–polyethyleneglycol bovine serum albumin (maleimide-PEG-BSA) derivative. The PEGylated nanoparticles are prepared using the

desolvation method. It is realized that the surficial modification with PEG could obviate the need for the surface-active RES interception and sequestration of nanoparticles. Further, the PEGylated nanoparticles are coupled with transferrin to render them site-specific carriers for brain targeting.

2. Materials and Methods

2.1. Chemicals, Reagents, and Instruments

The apocynin, bovine serum albumin, anhydrous ethanol crosslinker NHS-PEG-MAL-5000, and transferrin were purchased from Sigma Aldrich (St. Louis, MO, USA). The HPLC-grade ammonium acetate was purchased from VWR. The HPLC-grade water, methanol, and acetonitrile were purchased from Fisher Scientific (Waltham, MA, USA). The HPLC-grade glutaraldehyde (100%) was obtained from Alfa Aesar (Ward Hill, MA, USA). The Millipore Milli-Q Plus apparatus was used to procure the ultrapure water. All other chemicals used in this study were of analytical grade. Traut's reagent (2-Iminoethanol) and Ellman's reagent were obtained from Pierce (Rockford, IL, USA). The PD-10 and Sephadex™ G-25 M columns were from GE Healthcare. Lyophilizer, centrifuge (Eppendorf 5810R centrifuge, Thermo Scientific Sorvall RC 6+), zetasizer (Malvern), HPLC (Thermo Fischer, Waltham, MA, USA), sonicator, and rotaevaporator (Rotaevapor Buchi, R-210) instruments were used in this study.

The rat brain microvascular endothelial cells (#R1000) and rat astrocyte cells (#R1800) along with rat endothelial cell medium (#1021), bovine plasma fibronectin (#8248), and astrocyte medium (#1831) were purchased from ScienCell. The rat macrophage colony-stimulating factor (#300-523P) was purchased from Gemini. The poly-D-lysine hydrobromide (#P7280) and lipopolysaccharides from *Escherichia coli* O127:B8 (#L4516), Evans blue dye (#E2129), and absolute ethanol were purchased Sigma. The B-27 supplement (50×) and MTT (3-(4,5-dimethylthiazol-2-yl)-2,5-diphenyltetrazolium bromide) (#M649 4) were purchased from Thermo Fisher (Waltham, MA, USA) (<https://www.thermofisher.com/us/en/home.html>, accessed on 19 December 2022). The 6.5 mm transwell plates with 3.0-µm-pore polycarbonate membrane inserts (#3415) were purchased from Corning.

2.2. Formulation of Tf-Conjugated, Apocynin-Loaded Albumin Nanoparticles (Tf-apoANPs)

The Tf-conjugated BSA nanoparticles were formulated in three steps [12,24]. In the first step, apocynin-loaded albumin nanoparticles (apoANPs) were prepared using a modified desolvation method [25,26]. Briefly, 10% BSA (*w/v*) in HPLC-grade water was stirred (at 600 rpm) with 7.5% of apocynin (*w/v*) at room temperature for drug absorption onto albumin. After 1 h of continuous stirring, the pH value was adjusted from 7.5 to 8.5 using 0.1 M NaOH. The mixture was then desolvated through the addition of a suitable amount of ethanol, using a peristaltic pump at a rate of 1 mL/min under stirring (at 600 rpm). The ethanol addition was sustained until reaching turbidity and the residual ethanol was removed using a rotary evaporator at 4 °C. Then, the formulated apocynin-loaded nanoparticles were stabilized via crosslinking with an 8% glutaraldehyde solution for 24 h. The nanoparticles in solution were ultra-centrifuged (Sorvall LYNX 6000 Superspeed Centrifuge) at 36,288 × *g* for 40 min.

Secondly, the 2-iminoethanol solution was added to bind a sulfhydryl group to the transferrin. Briefly, the transferrin was dissolved in phosphate buffer (1 mg/mL at pH 8.0) and incubated with 12.8 µL (50.85-fold molar excess) of 2-iminoethanol solution (6.9 mg in 1.0 mL phosphate buffer, pH 8.0) in the dark for 2 h at 20 °C under constant shaking (500 rpm). Thereafter, the thiolated transferrin was purified using PD-10 and Sephadex™ G-25 M columns using phosphate buffer (pH 8.0) as the eluent.

Thirdly, the NHS-PEG-MAL-5000 solution with a 10-fold molar excess was introduced to the nanoparticles to activate them via cross-linking. To conjugate the NPs, 500 µL of thiolated and purified transferrin solution was added to 500 µL of reactive BSA NPs. The mixture was incubated under shaking for 24 h at room temperature. The thiolated transferrin excess was removed via two-fold nanoparticle centrifugation, dispersed in

water, and lyophilized. The precipitate obtained from the centrifugation was washed with pure water three times and then freeze-dried with the addition of 50 mg of mannitol to obtain a brownish fine powder of Tf-conjugated apoANPs. For further characterization, a stock suspension of NPs was used. Similarly, the drug-free ligand-conjugated empty albumin nanoparticles (tf-EANPs) were also prepared.

Two separate approaches were utilized to redisperse the lyophilized apoANPs, namely physical shaking and sonication [27]. The manual shaking method was applied using a weighed quantity of lyophilized NPs with phosphate-buffered saline at pH 7.4. The nanosuspension was subject to gentle shaking for 2 min to redisperse the solution and then immediately measured for its particle size using a Malvern zetasizer [28]. After gentle shaking for 2 min, the nanosuspension was subjected to particle size measurements using the Malvern zetasizer. The micrometer-sized particles were considered non-dispersible. The sonication method was applied with lyophilized NPs in phosphate-buffered saline at pH 7.4 for 2 min using a bath sonicator and the redispersibility method.

Conjugation of Cy5.5 to BSA nanoparticles: The near-infrared (NIR) fluorophore Cy5 was labeled on BSA-NPs to investigate the in vivo distribution of NPs in brain injury models [29,30]. The BSA nanoparticles were conjugated to Cy5.5 according to the manufacturer's recommended protocol [29,30]. Briefly, a reaction between the BSA and the Cy5.5-NHS ester (Invitrogen, Carlsbad, CA, USA) at a molar ratio of 1:2 was performed in the dark at room temperature for 1 h. The unconjugated dye was removed via dialysis against phosphate-buffered saline (PBS) using a Slide-A-Lyzer membrane cassette (3500 MWCO) for up to 18 h at 4 °C. The dialyzed samples were filtered through a 0.2- μ m syringe filter to ensure their quality before use.

2.3. Characterization of the Nanoparticles

The mean particle size, particle size distribution, and zeta potential values of the nanoparticles were measured using the zetasizer (Malvern). The zeta potential is the electrical potential at the slipping plane. This plane is the interface that separates mobile fluid from fluid that remains attached to the surface. The particle size and zeta potential measurements were conducted on freshly prepared dispersions of nanoparticle stock suspension (1 mg/mL) in PBS at pH 7.4. The results were reported as average values from triplicate runs of three independent experiments for each sample. The structural morphology of the nanoparticles was determined using a field emission scanning electron microscope (SEM LEO 1530VP). For the SEM imaging, nanoparticles in ethanol (20 μ L) were placed and converted into powder on the surfaces of carbon substrates [31,32]. Prior to the analysis, the samples were placed onto metal stubs using double-sided adhesive tape, then sputter-coated with gold/palladium to make them electrically conductive and suitable for SEM imaging (EM JSM-7900F, JEOL). For the TEM analysis, 10–20 μ L of the NP solutions in ethanol was placed on a 200-mesh copper grid coated with carbon. The copper grid was allowed to dry for 2 h at room temperature before imaging (JEM-F200/F2). The FT-IR transmittance spectra of the nanoparticles were obtained using a Spectrum 100 FTIR spectrometer (PerkinElmer) [31–33]. The data were collected in the wavenumber range of 400–4000 cm^{-1} at a resolution of 1/cm. The ¹H NMR spectra of the BSA, tfMANPs, and cy5.5-tagged MANPs were recorded on a Bruker Avance II 400 MHz spectrometer in deuterated chloroform (CDCl₃) at room temperature.

To determine the characteristic preservation of the alpha helical secondary structure, the circular dichroism (CD) spectra from the BSA, tf-apoANPs, and cy5.5-tagged apoANPs and were recorded at a concentration of 500 μ g/mL in PBS buffer using a Dichroism spectropolarimeter (J-810, Jasco International Co., Ltd., Grand Blanc, MI, USA) [1,2]. The far UV region was scanned between 190 and 240 nm. All data were buffer-corrected and converted to molar residual ellipticity (MRE) values. The MRE was calculated by $[\theta] = \theta \times m/c \times nr \times l$, where θ is the MRE in millidegrees, m is the molecular weight in g/mol, c is the concentration in mg/mL, l is the path length of the cuvette in cm, and nr is the number of amino acids in the peptide.

2.4. Entrapment Efficiency and Loading of Apocynin in Tf-Conjugated apoANPs

The amount of apocynin entrapped in the albumin nanoparticles was quantified using a validated HPLC method. The quantity of drug encapsulated was measured through indirect means, by quantifying the amount of apocynin in the supernatant obtained after ultracentrifugation. Further, the supernatant was dialyzed (20 kDa) to remove the traces of proteins. Briefly, 5 mL of supernatant was transferred into a dialysis cassette (10 mL, cutoff 20 kDa) and then the cassette was placed in a 200 mL beaker with HPLC-grade water. Before putting the sample in the dialysis cassette, the membrane of the cassette was hydrated with water. The medium was stirred at 250 rpm overnight, and 1 mL of the dialysis medium was withdrawn for the HPLC analysis [26,34]:

$$\% \text{ encapsulation efficiency} = \frac{(\text{total apocynin} - \text{apocynin in the supernatant})}{\text{total apocynin}} \times 100$$

For the apocynin loading efficiency, known quantitative albumin nanoparticles were dispersed in purified water, which was added as needed. The nanoparticle suspension was sonicated for 30 min and filtered through a 0.25 μm membrane (Whatman[®] membrane filters with a nylon pore size of 0.2 μm and diameter of 25 mm) and quantified using the HPLC method [34]:

$$\text{Drug Loading R} = \frac{(\text{Weight of apocynin in nanoparticles})}{\text{total apocynin}} \times 100$$

2.5. In Vitro Apocynin Release from Nanoparticles

The in vitro release profile of apocynin from the Tf-conjugated apoANPs was investigated via a dialysis method using phosphate-buffered saline (PBS; 0.01 M, pH 7.4) as the release medium. Briefly, 1 mL of the apocynin solution or Tf-conjugated apoANP suspension (1 mg/mL) in PBS was added to a dialysis bag (MWCO 80,000 Da) and incubated in 200 mL of release medium at 37 °C at a shaking speed of 100 rpm. For certain time points, a 0.5 mL aliquot was withdrawn (0 to 72 h) and replaced with an equal volume of fresh release medium. The samples were then subject to HPLC analysis, as described above, and shielded from light exposure during the process. These samples were analyzed in triplicate.

Cell culture 2.2.1. Astrocyte and endothelial cells:

The astrocyte and rat brain microvascular endothelial cells (RBMECs) were cultured according to the manufacturer's recommendations. Briefly, cryopreserved astrocytes were seeded on a 2 $\mu\text{g}/\text{cm}^2$ poly-D-lysine-coated flask to initiate the culture. The confluent cultures were further expanded for three population doublings. Finally, the astrocytes were harvested for the transwell culture. The cryopreserved RBMECs were seeded on a 2 $\mu\text{g}/\text{cm}^2$ fibronectin-coated flask to initiate the culture. Similarly, the confluent cultures were further expanded for three population doublings. Finally, the RBMECs were harvested for the transwell culture.

2.6. MTT Assay

The primary neurons were isolated from the cortices of rat embryos as previously described [34–36]. The cells were cultured in a 96-well plate in complete neurobasal medium for 7 days and then challenged with 100 ng/mL of a lipopolysaccharide and apocynin-free drug or apocynin nanoconjugate for 48 h, after which the cell viability was measured with an MTT assay. The media from each well were removed and replaced with a medium containing 5 mg/mL of 3-(4,5-dimethylthiazol-2-yl)-2,5-diphenyltetrazolium bromide (MTT) solution. The plates were incubated for 4 h at 37 °C followed by the removal of the MTT solution and addition of dimethyl sulfoxide (DMSO). The plates were cooled to room temperature and read on a plate reader at 570 nm. The percentages of viable cells were calculated using a standard curve assay and normalized to the control cells.

2.7. NO Measurement

The primary cortical neurons were cultured in a 24-well plate and treated with the PBS vehicle, 100 ng/mL of lipopolysaccharide, 100 mM or 200 mM of apocynin, and nanoparticle conjugate for 4, 24, or 48 h and then examined for their nitric oxide (NO) production. The NO measurements were conducted in real time with a World Precision Instruments Free Radical Analyzer TBR4100/1025 as previously described [35,37]. Briefly, after polarizing the ISO-NOP NO probe until the current reached a steady baseline value, the probe was calibrated via the decomposition of the photoactivatable nitric oxide donor S-nitroso-N-acetylpenicillamine, N7892, N7927 (SNAP). The current was then converted to the NO concentration using this calibration curve. The measurements of NO release by the neurons were performed by inserting the NO probe directly into cultured cells until the response reached a steady state.

2.8. Transwell Migration Assay

A transwell migration system was used to model the blood–brain barrier in vitro and examine the ability of nanoparticles to cross the BBB. The transwell system was prepared similarly to the previously described endothelial astrocyte coculture models [35,38,39]. Evans blue dye extravasation was performed to confirm the integrity of this in vitro model [39,40]. Briefly, 3.0 µm pore inserts were coated in 2 µg/cm² of fibronectin (overnight at 37 °C) to ensure the optimal adhesion of the cells. The inserts were inverted and primary rat astrocyte cells (#R1800, ScienCell) were seeded at a density of 5000 cells/cm² onto the underside of the transwell inserts and cultured in this manner for 2 h, with the medium being supplemented every 15 min to ensure attachment. After 2 h, the insert was inverted and rat primary brain microvascular endothelial cells (RBMECs, #R1000, ScienCell) were seeded at a density of 10,000 cells/cm² onto the surface of the transwell insert. After 7 days of culture, the nanoparticles were suspended in the endothelial medium and added to the upper chamber of the insert. Next, 25 µL of the medium was removed from the lower chamber at 0.5, 1, 2, 4, 24 h, and 7 days. Every time the medium from the lower chamber was removed, the upper chamber was supplemented with the equivalent volume to maintain the osmotic pressure.

The transmigration of the NPs across the BBB was calculated from the following equation:

$$\% \text{ of NPs in basal chamber} = \frac{\text{Fluorescence of NP at time } t \text{ in basal chamber}}{\text{Fluorescence of the Total Np in basal chamber}} \times 100$$

2.9. In Vivo Biodistribution of Targeted Tf-MANP in Blast TBI Rat Model

Animals: Ten-week-old male Sprague–Dawley (Charles River Laboratories, Wilmington, MA, USA) rats weighing 350 ± 50 g were used in accordance with protocols approved by the Rutgers University Institutional Animal Care and Use Committee (IACUC approval: PROTO201900142). The animals were housed with free access to food and water in a 12 h dark–light cycle at 22 °C. The rats were divided into four groups ($n = 5$; sham controls, the blast group, and two treatment groups exposed to a moderate blast of 180 kPa). The sampling points for the minocycline (3 h) and targeted nanoparticles (24 h) were chosen because the half-life of minocycline is 2–3 h in rat models and because of the extended systemic circulation period of targeted nanoparticles [41,42].

Blast injury: The rats were subjected to a single blast wave at the Center of Injury Biomechanics, Materials, and Medicine (New Jersey Institute of Technology, Newark, NJ, USA) in a 9 inch square cross-section shock tube, as described previously [43–46]. The principal animals used in this study were rats, with 4–5 animal in each experimental group (power value of 0.8, $\alpha = 0.05$) based on a power analysis. Before the blast exposure, all animals (controls, blast, blast + treatment) were anesthetized with 5% isoflurane, then released into a chamber containing 95% air and 5% CO₂. The rats were placed horizontally inside the shocktube (in a 6-m-long shock tube with a 9 inch square cross-section) located 2.8 m from the point where the shockwave was generated at one end of the tube and 3.05 m

from its exit. The rats were strapped securely to the aluminum plate using a cotton cloth wrapped around the body. The cloth provided no protection against the shockwave but prevented excessive motion of the head. The pressure waveform was recorded using PCB Piezotronics 134A24 sensors (Depew, NY, USA) at the 1.0 MHz sampling frequency for a duration of 5 ms. The rats were subjected to a single shock wave with a moderate blast of 180 kPa. The sham control rats received anesthesia and noise exposure without blast exposure, i.e., anesthetized animals were placed next to the shock tube and then a single blast was applied. Following the blast injury, the animals were closely observed for any signs of apnea or loss of motor coordination, and the modified neurological severity score (NSS) values were evaluated five minutes post-exposure. None of the animals included in this study displayed NSS values that differed from the sham animals.

Treatment regime: Targeted nanoparticles and free minocycline were intravenously injected at a dose of 3 mg/kg 4 h after exposing the rats to a single moderate blast (180 kPa). The samples were collected after 3 h and 24 h for the minocycline- and nanoparticle-treated groups, respectively.

Immunofluorescence Staining

The blast TBI rats were injected with fluorescently labelled targeted nanoparticles and non-targeted nanoparticles in the tail vein [44]. After 4 h, the brain was harvested and fixed with 4% paraformaldehyde for 24 h, incubated in a 30% sucrose solution for 72 h, and then stored at 80 °C until sectioning [47,48]. After blocking with 10% donkey serum for 1 h at room temperature, the sections were incubated with microglia and macrophages (rabbit anti-Iba1, Wako Laboratory Chemicals #019-19741, 1:2000, overnight at 4 °C), astrocytes (rabbit anti-GFAP, Dako Z0334, 1:5000, overnight at 4 °C), or neurons (mouse anti-beta III tubulin, Alexa Fluor® 488, Abcam #169556, 1:600, 4 h at RT). The rabbit primary antibodies were detected using Alexa Fluor® 488 goat anti-rabbit serum (LifeTechnologies, 1:500, 1 h at RT). The coverslips were mounted using Dako fluorescence anti-fade mounting media. The sections were washed and incubated with secondary antibodies for 1 h. The sections were washed and the images were captured using a Zeiss Axiovert 200 M microscope.

2.10. Statistical Analysis

The statistical analysis was performed using Graphpad Prism 5 software. The data are presented using means \pm SDs. The linear regression was computed using the least squares method and was used to produce calibration curve and correlation coefficient. The statistical analysis of the linearity of the curve was conducted through an analysis of variance (ANOVA). The statistically significant results indicated that not all means in the group were equal, which were further analyzed with Tukey's post-hoc honest significance tests for multiple comparisons of pairs. In both the bar and line graphs, the data are presented as means \pm the standard error from the mean (SEM). The threshold for statistical significance was $p \leq 0.05$ (* $p \leq 0.05$, ** $p \leq 0.01$, and *** $p \leq 0.001$). A statistical analysis was performed using the Rcmdr package in R software.

3. Results

In preparing the nanocarrier systems, the following factors should be considered: the physicochemical stability, biodegradation rate, drug entrapment efficiency, drug release kinetics, and brain-targeting capability. In addition, the pharmaceutical carriers can be designed as sustained release formulations [12]. Albumin is one of the most commonly used matrices for the preparation of particulate-based delivery systems, which can range from micrometric to nanometric in size [49]. The protein NPs were obtained via the known process of desolvation [50] which can be achieved through the precise addition of a desolvating agent (ethanol or acetone) to an albumin solution at an optimum pH for an optimal size, involving encapsulation with continuous stirring until reaching turbidity. A reduction in the solubility of the albumin after the phase separation in water during the desolvation process resulted in nanoparticle formation.

3.1. Apocynin-Loaded Albumin Nanoparticles (apoANPs)

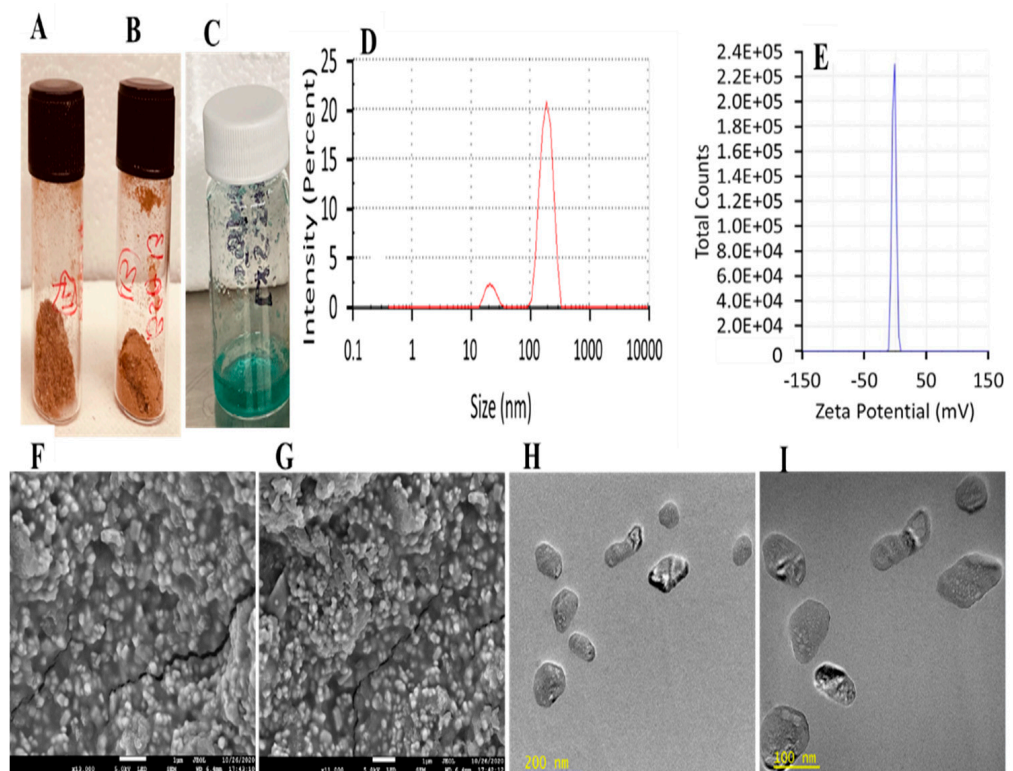
Our formulation for apocynin-loaded albumin nanoparticles (apoANPs) is based on the modified desolvation method [25]. Numerous studies have reported on albumin-based drug-loaded nanocarriers with chemical crosslinking agents such as glutaraldehyde [51,52]. In our study, parameters such as the pH level (between 7.0–9.0) and the amount of ethanol added were varied to optimize the particle size. The initial particle size was at a higher range (>275 nm), although by the end of the ethanol addition the particle size stabilized and became reproducible after crosslinking with glutaraldehyde, the removal of ethanol, and freeze drying occurred. Further, with 10% *w/v* BSA and a 1:1.3 ratio of BSA to ethanol, a supreme yield of 68.9% was attained. The particle sizes were higher when pH was <7.0 but pH range of 7.0–9.0 produced uniformly sized albumin nanoparticles. Further, when the ratio of BSA to ethanol was 1:2.5, the yield was higher than with the 1:5 ratio. Afterward, at the 1:2.5 ratio of BSA to ethanol, the particle size also enlarged to 320 nm, which was prior to the ethanol removal. After the ethanol removal and freeze-drying, the particle size was condensed to be the optimal and the PDI indicated a nearly homogenized nanoparticle system.

Additionally, the nanoparticles were stabilized by crosslinking lysine and guanidino side chains of albumin with glutaraldehyde [25], and the rigidity of the nanoparticles decreased with the particle size. With our method, the hydrophobic apocynin aggregates in the aqueous solution and networks with the hydrophobic regions of the BSA, forming nanoparticles, which are stabilized with glutaraldehyde by cross-linking the surface amino groups of the BSA [53]. The NH₂ from BSA molecules reacts with the carbonyl group of the glutaraldehyde to form the -N=C- bond via the removal of a molecule of water. In this way, the nanoparticles of albumin crosslinked with glutaraldehyde are formed [54]. The glutaraldehyde crosslinked with albumin shows no toxicity, and the obtained NPs are non-toxic after the removal of free glutaraldehyde via centrifugation [32].

The primary aim is to provide the desirable bioavailability at a significantly lower concentration to achieve maximum bioavailability for the apocynin in the injured brain using novel apoANPs. Our proposed research on TfR (transferrin receptor)-targeted apoANP nanoparticles will exploit both receptor-mediated endocytosis in the vasculature and transiently leaky BBB conditions (as confirmed by our published article using a blast TBI model) to enhance the bioavailability at the injury site and reduce the toxicity of the drug [43,44]. Transferrin-appended albumin nanoparticles were prepared by coupling the transferrin protein to the distal end of the PEG chain, as reported previously, with slight modifications [49]. In our study, the possibility of using covalently bound, transferrin-modified nanoparticles was investigated to transport drugs across the BBB; hence, the transferrin was conjugated with the NHS-PEG-MAL to BSA NPs. The covalent attachment of the ligands as in the present study enables the manufacture of stable systems. This method is advantageous over the simple adsorption of the antibody onto the nanoparticle surfaces, as employed in earlier studies. The coupling of transferrin slightly increased the size of the nanoparticles from about 160 to about 185 nm. Other authors also reported comparable small nanoparticle size increases after the attachment of transferrin [24]. In order to evaluate the extent of Tf conjugation in the PEGylated albumin nanoparticles, the coupling efficiency of Tf was estimated using a quantitative analysis that was performed after the separation of the unconjugated transferrin. The average number of Tf molecules per thousand PEG chains was calculated by assuming that the molecular weight of Tf is 80,000. It was found that nearly 3.5% of the total PEG chains were linked to Tf molecules.

The nanoparticles were freeze-dried with 0.05% mannitol, resulting in a powder that could also be dispersed in PBS or 0.9% saline (Figure 2A,B). Evenly sized nanoparticles allow augmented cellular interactions and possess enhanced toxicity [55], hence, the size of the nanoparticles plays a vital role in their cell interactions and toxicity. The PDI and mean particle size of the nanoparticles were measured by DLS in PBS at pH 7.4. The results showed a well-dispersed colloidal system of apoANPs with a mean particle size and polydispersity index of 135.4 ± 5 nm and 0.275 ± 0.01 , respectively, with a distribution

range of 140–250 nm (Figure 2C). The index of the particle size distribution is stated as the PDI. It has an impact on the pharmacokinetic parameters and the therapeutic efficacy of the medicated NP formulations through values of 0 to 1. PDI values lower than 0.2 specify a homogenous dispersion, while those greater than 0.2 indicate a heterogeneous one. An unsatisfactory particle size (PDI > 0.5) can affect the surface area of the NPs and their absorption, in turn affecting the pharmacokinetic parameters and therapeutic efficacy of the formulation. The ligand-conjugated tf-apoANPs exhibited a mean particle size and polydispersity index of 153.5 ± 3.4 nm and 0.203 ± 0.5 , respectively (Figure 2D). Studies have shown that the cellular internalization and cytotoxicity depend on the zeta potential of the nanoparticles [28,56]. Freeze-drying may increase the particle size of the nanoparticles; hence, we checked the redispersibility of the particles after lyophilization via shaking and sonication. In our study, most of the NP formulations had PDI values < 0.5, pointing to their narrow size distribution. The morphologies of freeze-dried apoANPs and tf-apoANPs were assessed via FE-SEM, and are shown in Figure 2E,F. Both types of synthesized NPs had nearly spherical morphologies, which to some extent were connected to each other, with an average size of 120 ± 30 nm for the apoANPs and 148 ± 6 nm for the tf-apoANPs synthesized at pH 7. Furthermore, the tf-apoANPs showed a more even distribution compared to the apoANPs. The TEM analysis showed that the apoANP and tf-apoANP samples contained spherical particles measuring 120–180 nm in diameter (Figure 2G,H), which were compared using SEM and zetasizer analyses.



J Sample	Particle Size (nm)	PDI	Zeta Potential (mv)	Entrapment efficiency (%)
apoANP	165.4±3.2nm	0.245±0.8	-3.02±1.2mv	73.4±0.1%
Tf-apoANP	183.5±5nm	0.293±1.5	-5.74±3.4mv	68.4±2.3%

Figure 2. Characterization of apoANPs and tf-apoANPs. Freeze-dried samples of (A) apoANPs,

(B) tf-apoANPs and (C) Cy5.5-conjugated tf-apoANPs. Particle sizes of (D) apoANPs and (E) tf-apoANPs. Representative SEM images of (F) apoANPs (magnification = 25,000 \times) and (G) tf-apoANPs (magnification = 30,000 \times). Representative TEM images of (H) apoANPs (magnification = 26,000 \times) and (I) tf-apoANPs (magnification = 26,000 \times). (J) Table listing the particle size, PDI, zeta potential, and entrapment efficiency values of apoANPs and tf-apoANPs (data expressed as means \pm SD ($n = 3$), statistical significance ($p < 0.05$)). PDI: Polydispersity index.

The zeta potential quantifies the degree of repulsive interaction between nanoparticles and depends on the concentrations of the polymer and the incorporated drug. Specifically, the zeta potential is calculated as the difference in electrical potential between the surfaces of the nanoparticles and the bulk-surrounding medium [57]. The zeta potential information is helpful in predicting the storage stability of colloidal dispersions [27]. In our study, the apoANPs and tf-apoANPs exhibited anionic charges of -2.52 ± 1.2 mV and -3.14 ± 3.4 mV, respectively. Albumin comprises free carboxyl and amine groups, both of which could be utilized for covalent modification. In general, albumin shows a negative zeta potential (high anionic) at physiological pH and saline levels. Further, negative albumin (nearly neutral) can also be obtained via surface modifications of the anionic groups [23].

We obtained the FTIR spectra of BSA, transferrin, apocynin, apoANPs, and tf-apoANPs (Figure 3). The FTIR spectra of BSA displayed several distinguishing peaks at 3317 cm^{-1} arising from amine groups (N-H stretching vibration); a peak in the amide bond at 1657 cm^{-1} was attributed to C=O stretching vibration (amide I band), with another attributed to mixed vibrations of N-H bending and C-N stretching (amide II band) at 1536 cm^{-1} [53].

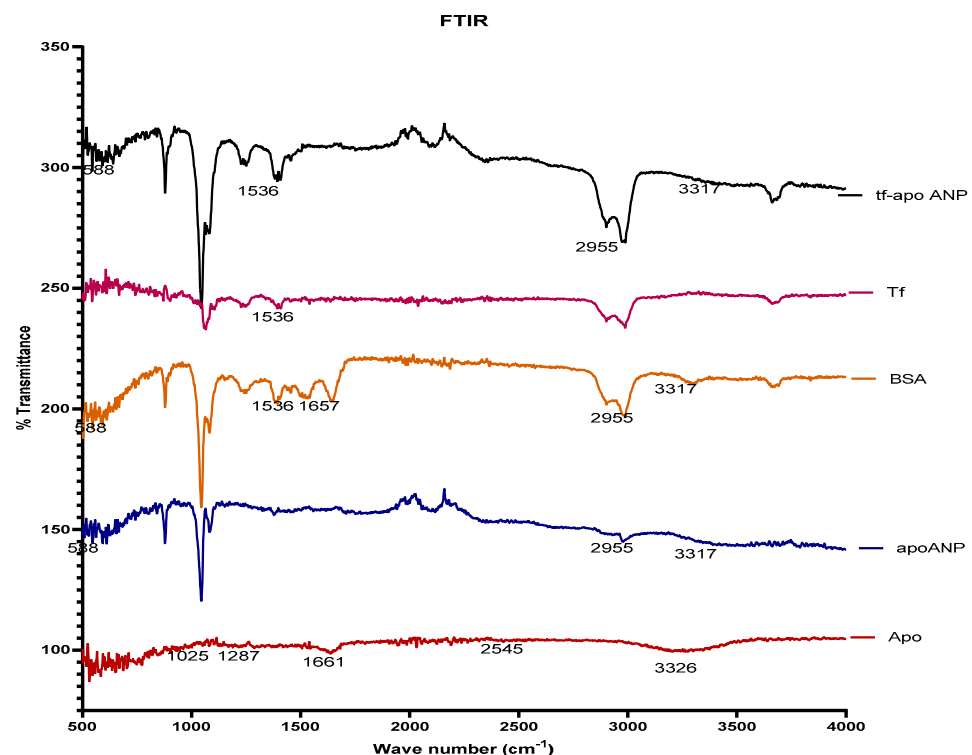


Figure 3. FTIR spectra of BSA, transferrin apocynin, apoANPs, and tf-apoANPs.

The FT-IR spectra results are shown in Figure 3. The spectrum of pure apocynin showed a stretching vibration at 3326 cm^{-1} that corresponded to the hydroxyl groups, while the band at 1661 cm^{-1} was attributed to the C=O of the conjugated ketone. The peak at 1025 cm^{-1} corresponded to symmetrical axial deformation to C-O of the ether bonds

and the peak at 1287 cm^{-1} corresponded to axial and angular deformation to $\text{C}-\text{C}(=\text{O})-\text{C}$. The FT-IR spectrum of BSA showed a broad band at 3317 cm^{-1} arising from amine groups (N-H stretching vibration); the peak of the amide bond at 1657 cm^{-1} was attributed to the $\text{C}=\text{O}$ stretching vibration (amide I band) and to the mixed vibration of N-H bending and C-N stretching (amide II band) at 1536 cm^{-1} . The spectrum of BSA nanoparticles containing apocynin showed stretching vibration at 3317 cm^{-1} , which may be attributed to the N-H stretching vibration from amine groups of BSA and O-H from apocynin. The peak shift to 1663 cm^{-1} corresponded to the superposition of the bands to the $\text{C}=\text{O}$ of apocynin (1661 cm^{-1}) and BSA (1657 cm^{-1}); the peak at 1025 cm^{-1} corresponded to a symmetrical axial deformation to C-O of the ether bonds of the apocynin, while the peak at 1287 cm^{-1} corresponds to axial and angular deformation to $\text{C}-\text{C}(=\text{O})-\text{C}$ of the aromatic ketones present in the apocynin. The results showed the absence of chemical interactions between BSA and apocynin, suggesting that the nanoencapsulation process does not alter the chemical structure of the drug [58]. The presence of the relevant peaks in each nanoparticle confirmed that the apocynin was encapsulated in the BSA nanoparticles.

The BSA, transferrin, apocynin, and tfMANP conjugates were characterized via proton nuclear magnetic resonance spectroscopy ($^1\text{H-NMR}$) to confirm the successful synthesis. The $^1\text{H-NMR}$ analyses were recorded on a Bruker DRX-600 Avance III spectrometer with deuterated chloroform (CDCl_3) as the solvent at room temperature. The samples (1 mg of each) were dissolved in 1 mL of CDCl_3 and the products were assessed using an NMR spectrometer. The results showed that there was no specific peak of apocynin in the nanoparticles, which confirmed that there was no chemical interaction and only a physical mixture of nanoparticles and BSA. However, there was a peak at 3.8, which confirmed the ligand's conjugation to the nanoparticles, corroborating the FTIR results (Figure 4).

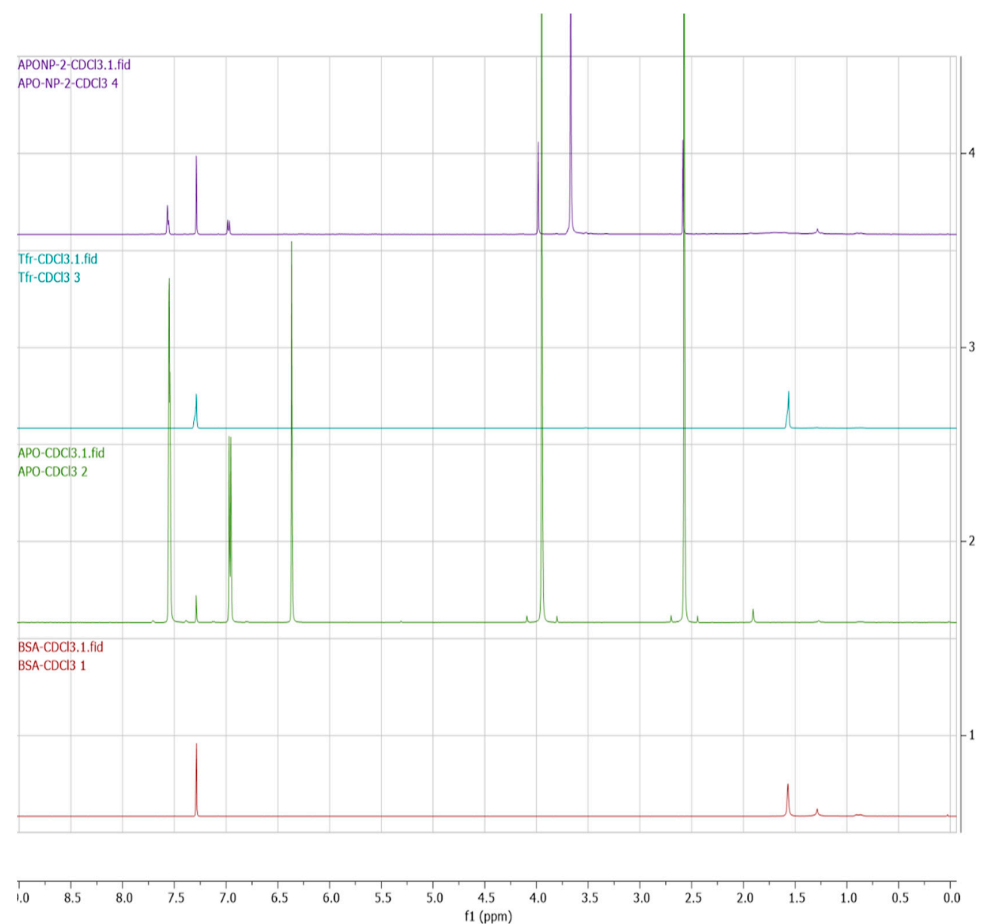


Figure 4. NMR spectra of BSA, transferrin, apocynin, and tf-apoANPs.

3.2. Entrapment Efficiency and In Vitro Release Study

For an optimal drug delivery system, the encapsulation efficiency and in vitro drug release are indispensable parameters to be analyzed [59,60]. We observed that the HPLC method is appropriate for the estimation of apocynin from nanoparticles. The encapsulation efficiency of apocynin was determined indirectly from the supernatant via centrifugation to estimate the free apocynin [34]. Almost $59.4 \pm 1.7\%$ and $0.45 \pm 0.06\%$ of the entrapment efficiency and drug loading rate, respectively, were determined ($n = 3$). The in vitro release profiles of apocynin and apocynin-loaded nanoparticles are shown in Figure 5. At the beginning, the spurt release of apocynin was observed after 30 min ($22.9 \pm 1.3\%$), and the gradually an increased release until 24 h in dissolution medium as compared to free apocynin ($61.5 \pm 2.4\%$). The free drug adsorbed onto the NP surfaces and the drug was entrapped near the surface, which may account for the initial burst release. It is suggested that the surface-implanted apocynin would be released earlier than from inside the nanoparticles. Within 24 h, approximately $70.3 \pm 2.9\%$ of the apocynin was released as compared to the free apocynin ($98.3 \pm 1.8\%$). Then, the release rate gradually stabilized to a sustained release rate from 24 h to 72 h, which can be attributed to the soluble nature and formation of interconnected pores on the surface and inside the albumin nanocarrier upon contact with the dissolution medium. Further, the NPs with glutaraldehyde crosslinking of the surface amino groups displayed slower drug release kinetics [53].

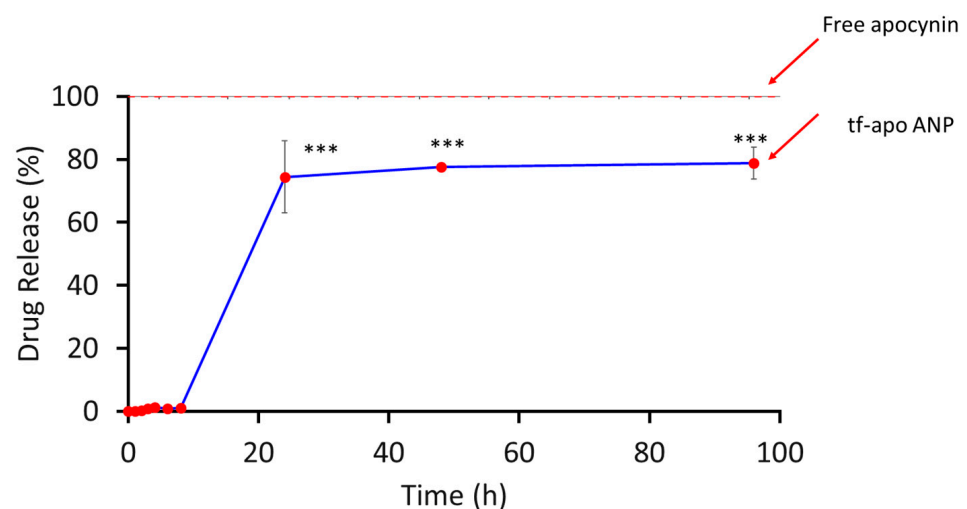


Figure 5. Drug release profile of apocynin-loaded albumin nanoparticles. The values shown here represent the SD ($n = 3$). A two-way ANOVA and multiple-comparison analysis were performed; *** $p < 0.001$.

3.2.1. MTT Analysis

The nanoparticle–apocynin conjugate improved the cell viability when loaded with apocynin concentrations ≥ 100 mM, whereas apocynin alone decreased the cell viability (Figure 6A). This result may have been due to the release kinetics of apocynin from the nanoparticle construct. These results also demonstrated that the nanoparticle–apocynin conjugate can outperform the free apocynin alone. In the case of L-glutamine-treated cells, the nanoconjugate showed a biphasic response that reduced the cell viability at lower concentrations and improved the cell viability at higher concentrations. This could be because of the slow release of apocynin and potential synergetic effect of both the albumin protein and apocynin to mitigate the L-glutamine-induced toxicity in the neurons (Figure 6B). Here, we report for the first time that apocynin-loaded albumin nanoparticles reduce neuronal death [61]. The overall data indicated that the synthesized APO-NPs have negligible toxic effects on neural cells and that their treatment in stressed conditions enabled the cells to hold their viability in comparison to APO alone.

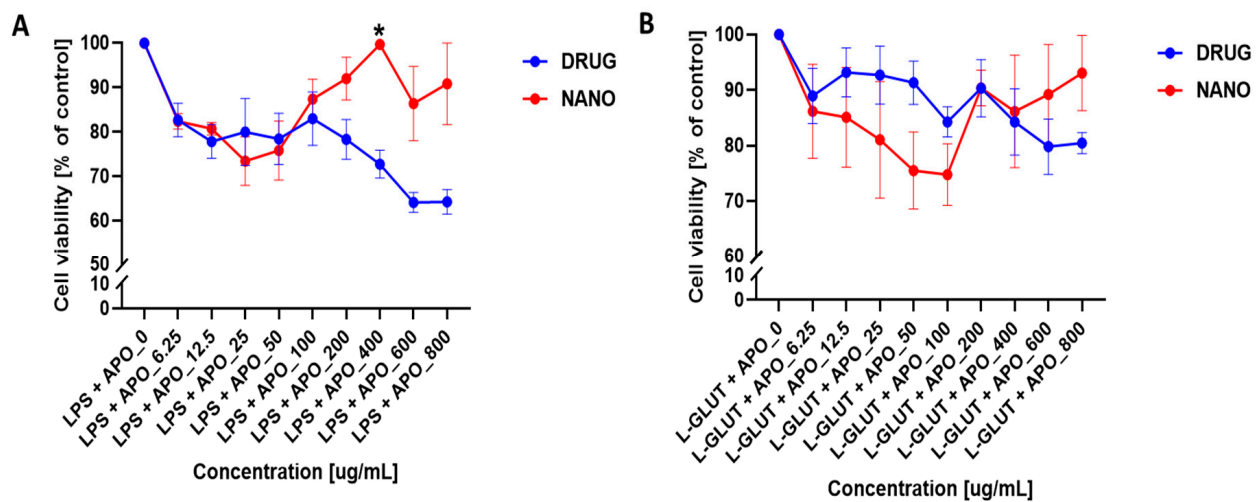


Figure 6. Cell viability assessment of apocynin and nanoparticle–apocynin conjugate treatments. Percentages of viable neuronal cells after treatment with increasing concentrations of apocynin alone (DRUG) or the nanoparticle–apocynin conjugate (NANO) for 48 h when combined with (A) 100 ng/mL lipopolysaccharide or (B) 100 µM L-glutamic acid are shown. The data were analyzed using a two-way ANOVA with Šidák’s multiple comparisons test. The results are presented as mean values (\pm SEM, N = 4 experiments). Significant difference are indicated by * $p \leq 0.05$.

3.2.2. NO Analysis

Since the half-life of nitric oxide (NO) is very short, in the order of a few seconds, we measured the real-time production of NO by neurons exposed to different apocynin and nanoparticle–apocynin conjugate concentrations for 4, 24, and 48 h. Here, 100 ng/mL of lipopolysaccharide and 200 mM of apocynin caused significant NO production after just 4 h of incubation (Figure 7A). At 24 h, only the nanoparticle-conjugated apocynin did not cause a significant increase in NO production, and the nanoparticles conjugated with 200 mM of apocynin caused NO levels comparable to the control (Figure 7B). By 48 h the NO production was significantly reduced by both drugs alone and by the nanoparticles to control levels (Figure 7C). As we noted when we compared the results at 4 and 24 h, the apocynin nanoconjugate at 24 h showed reduced NO production as compared to results at 4 h and for the free apocynin, which may have been because of the stability and degradation of the free apocynin and the slow release of apocynin from the nanoparticles to produce therapeutic effects at 24 h. In comparison, the apocynin nanoconjugate at 48 h reduced the NO production compared to the results at 4 h and for the free apocynin, which may have been because of the stability and degradation of the free apocynin and slow release of the apocynin from the nanoparticles to produce a therapeutic effect at 48 h. The nanoparticles loaded with apocynin significantly reduced the LPS- and L-glutamine-induced cell death and NO production compared to the control and free apocynin itself [61]. Previous results using apocynin also support our results in terms of the scavenging activity, confirming the better quenching of nitrite ions in the samples. Therefore, from the collective results, it can be concluded that cumulatively the APO-NPs showed a slightly better inhibition ability in comparison to APO alone [11]. The findings of this study demonstrate for the first time that apocynin treatments provide neuroprotection [9].

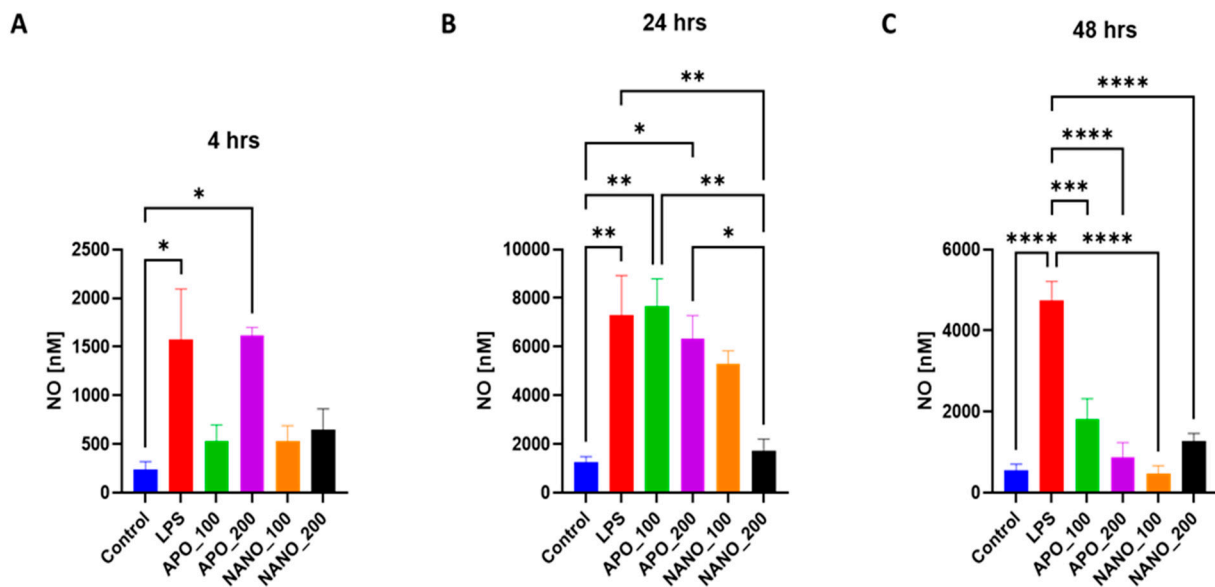


Figure 7. Measurement of NO production in injured neurons treated with the nanoparticle–apocynin conjugate. The primary cortical neurons were treated with either the PBS vehicle (control), 100 ng/mL of lipopolysaccharide, 100 mM of apocynin (APO_100), 200 mM of apocynin (APO_200), nanoparticles conjugated with 100 mM of apocynin (NANO_100), or nanoparticles conjugated with 200 mM of apocynin (NANO_200). The amounts of NO produced were measured at (A) 4, (B) 24, and (C) 48 h. The data were analyzed using a one-way ANOVA with Tukey’s multiple comparisons test. The results are presented as mean values (\pm SEM, N = 4 experiments). Significant differences are indicated by * $p \leq 0.05$, ** $p \leq 0.01$, *** $p \leq 0.001$, and **** $p \leq 0.0001$.

3.3. Transwell Analysis

To study the ability of nanoparticles to cross the blood–brain barrier (BBB), we used an RBMEC/astrocyte transwell coculture to model the BBB in vitro and to study the migratory response of the nanoparticles (Figure 8). Without perturbation to the BBB model, the nanoparticles began to significantly move across the BBB model after 4 h of incubation (Figure 9A). Our previous work [35] showed that 24 h of treatment with 20 mM of EtOH causes a significant increase in the permeability of the BBB transwell model; 20 mM EtOH is equivalent to a moderate dose of alcohol (>0.08% blood alcohol concentration). We saw significant movement of the nanoparticles after 24 h of EtOH treatment. The percentage of nanoparticles that crossed the barrier at 24 h following the EtOH treatment was greater than with no EtOH treatment (Figure 9B). This result demonstrates that nanoparticles can respond to injury by increasing their movement. The NPs showed an ability to cross the in vitro BBB. The percentage of NPs that crossed the BBB model reached $0.5 \pm 0.1\%$ after two hours of incubation and reached $7.7 \pm 0.8\%$ at 24 h, which was a 15-fold increase in movement. The percentage of NPs that crossed the BBB model when the model was challenged with 10 mM of EtOH reached $1 \pm 0.2\%$ after two hours of incubation and reached $9.9 \pm 1.1\%$ at 24 h, which was a 10-fold increase in movement. Damage to the BBB caused twice as many NPs to respond after 2 h of incubation and 1.3 times as many at 24 h. These results show that our transferrin-conjugated nanoparticles cross both the compromised and uncompromised BBB well. Our results were further corroborated by another study involving transferrin-conjugated nanoparticles crossing the BBB to respond to glioblastoma [62,63]. The mechanism of the enhanced efficacy of the nanoparticles with conjugated transferrin appears to be due to a higher cellular drug uptake [24].

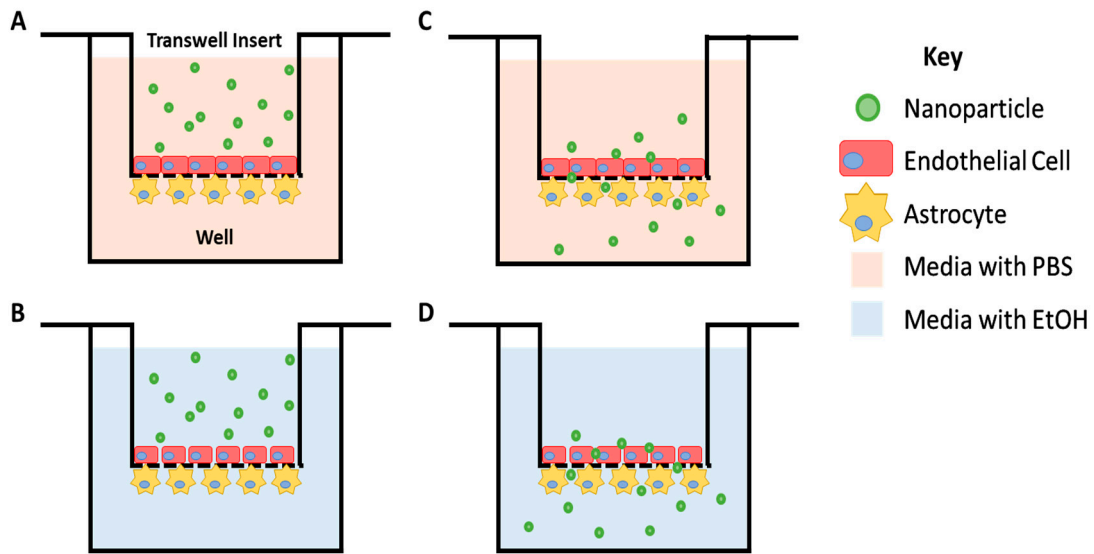


Figure 8. Cartoon depicting the transwell scheme. Primary rat brain microvascular endothelial cells were cultured on the 3 μm pore transwell insert while astrocytes were cultured underneath the insert. Nanoparticles were suspended in the basal medium (A) or a medium containing 20 mM of EtOH (B) and added to the transwell insert. (C,D) The movement of nanoparticles across this barrier, towards the well, was monitored over time.

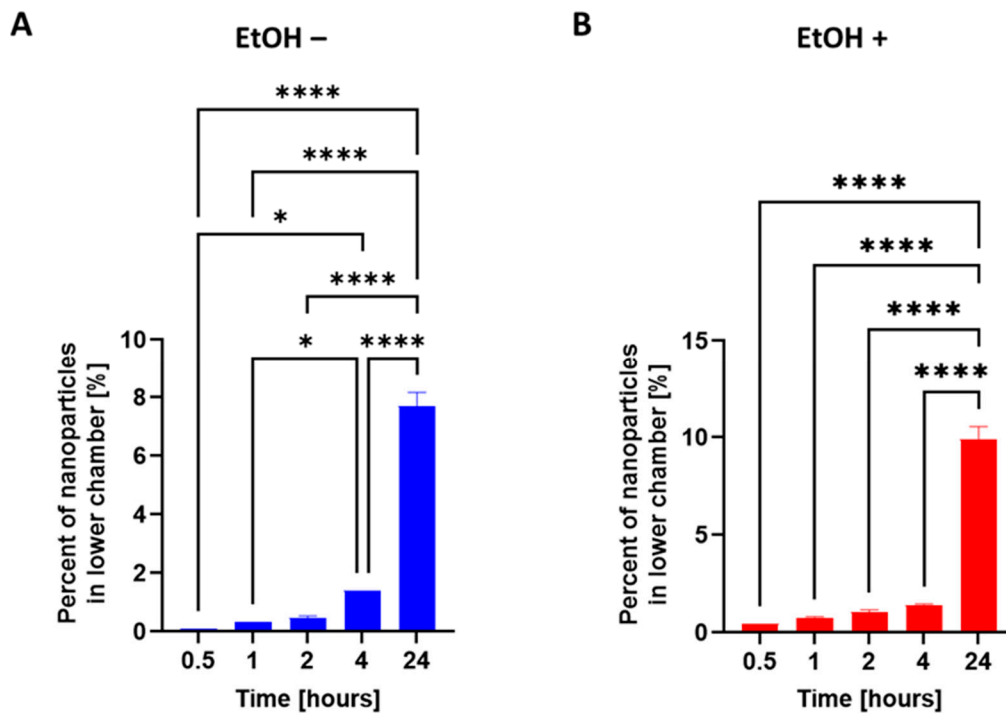


Figure 9. Nanoparticle migration through an in vitro model of the blood–brain barrier. The apical side of the model was treated with either the (A) PBS vehicle (EtOH –) or (B) 10 mM of ethanol (EtOH +) for 24 h, after which time a suspension of fluorescently tagged nanoparticles was added. The migration of nanoparticles was observed at 0.5, 1, 2, 4, and 24 h. The data were analyzed using a one-way ANOVA with Tukey’s multiple comparisons test. The results are presented as mean values (\pm SEM, N = 4 individual models). Significant differences are indicated by * $p \leq 0.05$ and **** $p \leq 0.0001$.

To study the morphology and behavior of the injured neurons exposed to free apocynin and nanoparticle-conjugated apocynin, we injured primary cortical neurons with 100 ng/mL of lipopolysaccharide for 48 h to cause visible changes to the neurite integrity. Following the injury, the neurons were treated with either 100 mM of apocynin or the nanoparticle–apocynin conjugate for 24 h. Although both the drug alone and the drug conjugated to nanoparticles ameliorated the effects of LPS damage by improving the structures of both the axons and dendrites, the drug alone caused neuronal clustering. The formation of neuronal clusters in the culture is the resulting response of neuronal cells to a stressful environment. The nanoparticle–apocynin conjugate did not cause the formation of large, compact clusters, and the culture results were comparable to the no-injury control (Figure 10).

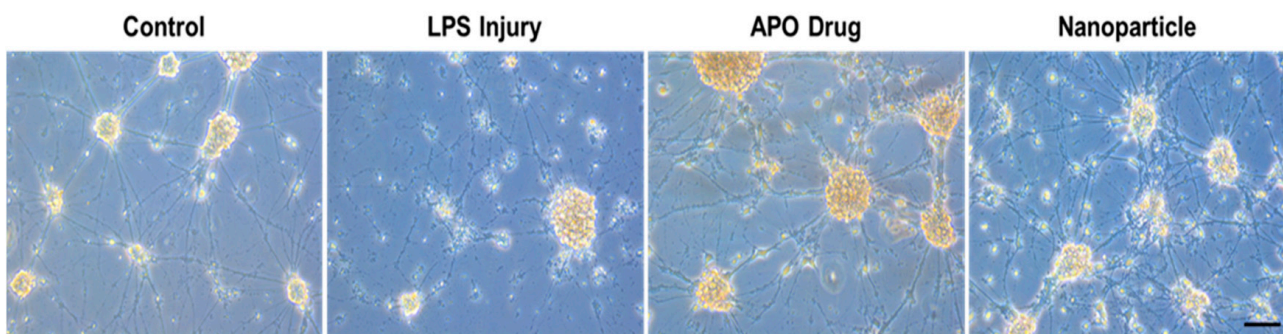


Figure 10. Effects of nanoparticle–apocynin conjugate treatment of injured neurons. Representative images of primary rat cortical neurons in the medium (control), after 48 h in 100 ng/mL of lipopolysaccharides (LPS injury) or 100 mM of apocynin (APO Drug), or in the nanoparticle–apocynin conjugate (nanoparticles) after 24 h of exposure to 100 ng/mL of lipopolysaccharides. The black bar represents 100 μm (20 \times magnification).

3.4. apoANPs and tf-apoANPs Crossed the BBB and Internalized in Parenchyma and Glial Cells

The CNS is well protected by the BBB [39,63] which not only maintains homeostasis but also hampers the systemic delivery of therapeutically important drugs from the blood to the brain [48]. The traditional approaches employed for enhancing drug concentrations in the brain, such as direct intracerebral drug injection or disruption of the BBB, are associated with high risks [63]. Biodegradable polymeric nanoparticles are some of the most promising drug and gene delivery systems that cross the BBB [48,64]. Nanoparticle formulations can encapsulate molecules with therapeutic value and enhance drug transport through the BBB in patients with ischemic brain injury [48]. In the present study, we investigated whether Cy5.5-conjugated apoANPs and tf-apoANPs localized after crossing the BBB. With non-targeted apoANPs and targeted tf-apoANPs, tissue confocal microscopy was used to observe the distribution of fluorescent signals for Cy5.5-conjugated apoANPs and tf-apoANPs (Figure 11). A large amount of Cy5.5-conjugated tf-apoANP fluorescence was observed in the cytoplasm or the vicinity of microglia and astrocytes of the hippocampus and thalamus in the rat bTBI model, which was significantly higher than in the rats treated with the non-targeted Cy5.5-conjugated apoANPs [48]. These results demonstrated that the apoANPs and tf-apoANPs could effectively mediate the brain targeting of nanoparticles and have potential for drug delivery to the brain [63].

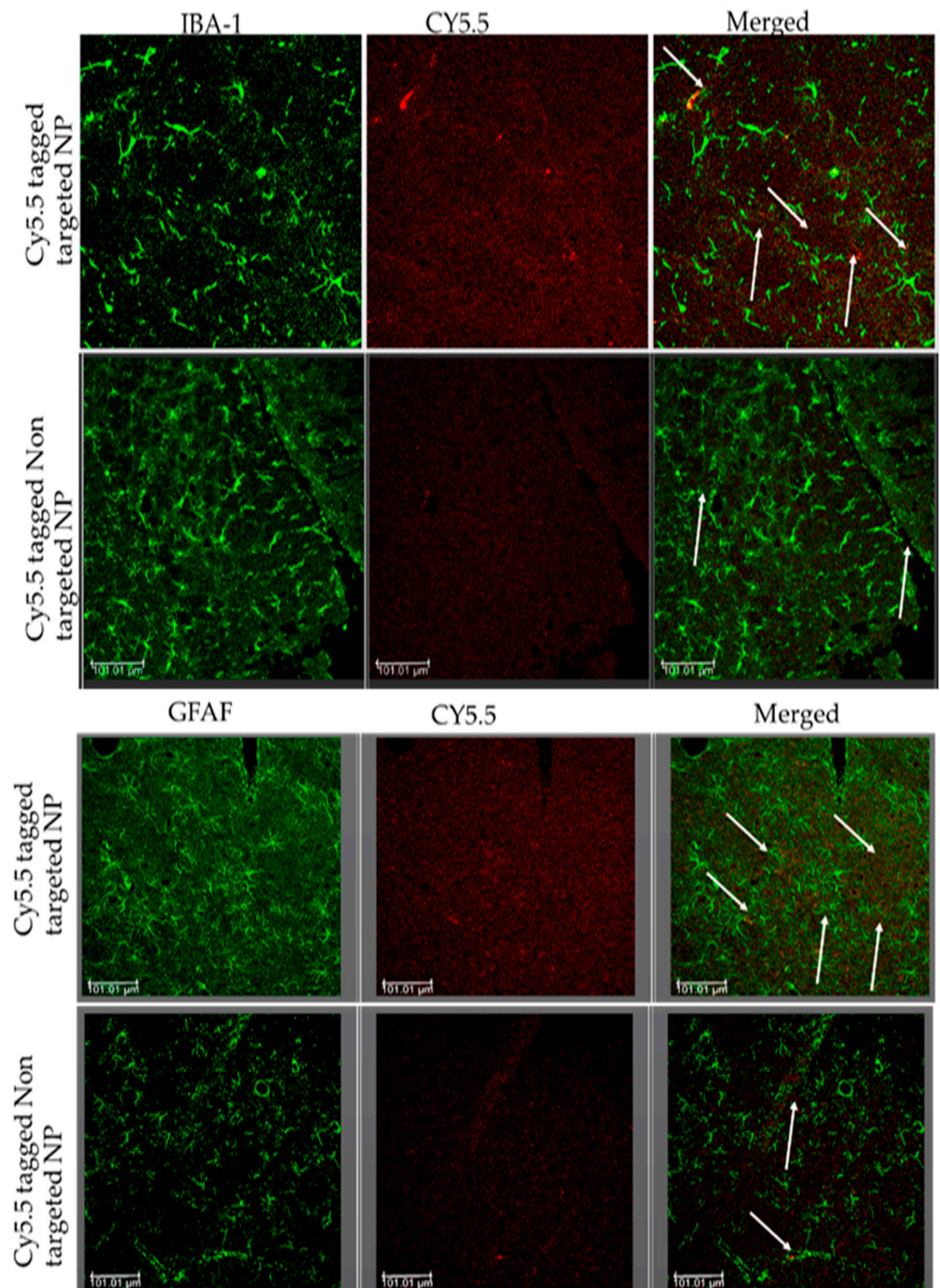


Figure 11. Nanoparticles internalized in the parenchyma and glial cells of the brain by crossing the BBB and via active targeting using transferrin receptors. The bTBI rats were intravenously injected with Cy5.5-conjugated apoANPs and tf-apoANPs and then sacrificed 6 h after the injection. The brain tissues were collected from 6 h after injections of Cy5.5-conjugated apoANPs and tf-apoANPs. The sections were observed under a confocal microscope. The distribution in the brain parenchyma and uptake of Cy5.5-conjugated apoANPs and tf-apoANPs (white) by the microglia and astrocytes are shown. Scale bar = 100 μm.

Transferrin receptors are reportedly present on the surfaces of diverse classes of cells, and the internalization of iron-saturated transferrin is controlled through receptor-mediated endocytosis [49]. Transferrin receptors are expressed on the luminal membranes of brain

endothelial cells and mediate the endocytosis of transferrin in NPs. The receptor-mediated endocytosis of transferrin from the blood to the brain is well documented [49]. The brain endothelial cells functionally belong to the polarized epithelium, with distinct apical and basal membrane domains (Beck et al., 1986). The endocytic pathway of transferrin in polarized epithelial cells has been the major focus of several reports [49].

There are different possibilities for how this transport of substances across the blood–brain barrier may be facilitated by polysorbate-80-coated nanoparticles: (1) NPs may adsorb at the endothelium, forming the blood–brain barrier and yielding a concentration gradient, leading to enhanced brain uptake of the delivered drug; (2) the surfactant may affect the blood–brain barrier’s integrity via the solubilization of membrane lipids; (3) nanoparticles may induce opening of the tight junctions; (4) the surfactant may inhibit the blood–brain barrier’s multidrug efflux system; (5) nanoparticles may be endocytosed into the brain endothelial cells and release their transported substances to be further delivered to the brain (Kreuter, 2004); (6) nanoparticles may be transcytosed through the endothelium forming the blood–brain barrier. It is possible that various mechanisms contribute to the brain’s uptake of drugs mediated by tf-apo nanoparticles.

4. Conclusions

Even though apocynin can cross the BBB, it cannot reach optimal concentrations in the brain parenchyma to produce a pronounced therapeutic effect. This is due to the short half-life of apocynin and the requirement for a higher administration dose to achieve a neuroprotective effect. As a preliminary approach, to increase drug availability in brain tissues, we endeavored to optimize the formulation parameters of transferrin-conjugated, apocynin-loaded albumin nanoparticles prepared using the desolvation method. Our study indicates that the developed formulation produced monodispersed, nanosized particles with higher entrapment efficiency, loading rate, stability, and sustained release profiles. All biomaterials involved in this nanoparticle formulation were already approved for clinical usage. The HPLC method we developed is precise, accurate, specific, and stable in the determination of apocynin. In vivo nanoparticle localization studies using a bTBI model and confocal fluorescence microscopy showed that the tf-apoANPs were successful in delivering relatively high amounts of nanoparticles to the brain parenchyma and glial cells compared to non-targeted nanoparticles. We also showed that the targeted nanoparticles particularly accumulated near microglia and astrocytes. The cytotoxic assays showed that the nanoparticles were non-toxic to the primary neurons. The free apocynin and the nanoformulation were evaluated for their neuroprotective effects against glutamate-induced excitotoxicity, as well as their anti-inflammatory potential in LPS/IFN-stimulated neurons. Here, we report for the first time that the novel apocynin-loaded nanoparticles reduce neuronal death. This study revealed that the apocynin-loaded nanoparticles markedly downregulated nitric oxide in LPS-treated neurons. The results collectively indicate the potential of the apocynin-loaded nanoparticles as highly effective therapeutic agents for neuroinflammation and oxidative disorders in the brain. However, more detailed in vitro and in vivo evaluations are needed to validate our findings. In a future study, we will evaluate the therapeutic efficacy of the targeted nanoparticles in a blast-induced TBI model in terms of the behavioral and neuroprotective aspects using a molecular analysis.

Author Contributions: Conceptualization, V.P.; methodology, V.P., M.K., X.L., A.R.R., A.A., S.V. and S.S.I.; software, V.P., M.K., X.L., A.R.R., A.A., S.V. and S.S.I.; validation, V.P., X.L., A.R.R., J.H., Y.Z. and N.C.; formal analysis, V.P., M.K., X.L., A.R.R., A.A., S.V. and S.S.I.; investigation, V.P.; resources, N.C. and Y.Z.; data curation, V.P., M.K., X.L., A.R.R., A.A., S.V. and S.S.I.; writing—original draft preparation, V.P.; writing—review and editing, V.P., M.K., X.L., A.R.R., A.A., S.V. and S.S.I.; supervision, N.C.; project administration, N.C.; funding acquisition, N.C. All authors have read and agreed to the published version of the manuscript.

Funding: This research was funded by the faculty seed grant (FSG), NJIT.

Institutional Review Board Statement: The animal protocol was approved by the Rutgers University Institutional Animal Care and Use Committee (IACUC approval: PROTO201900142).

Informed Consent Statement: Not applicable.

Data Availability Statement: Data is unavailable due to privacy or ethical restrictions.

Acknowledgments: We are grateful to the undergraduate students Samiksha Raman, Srijan Thota, Saisanjana Vellampalli, Yousef Hammouda, and Rashmi Venkatarama at the New Jersey Institute of Technology for their assistance in conducting the research work and preliminary studies. We also thank Vivek Kumar and his lab members for helping analyzing the data in the FTIR study.

Conflicts of Interest: The authors declare no conflict of interest.

References

1. Prins, M.L.; Alexander, D.; Giza, C.C.; Hovda, D.A. Repeated mild traumatic brain injury: Mechanisms of cerebral vulnerability. *J. Neurotrauma* **2013**, *30*, 30–38. [[CrossRef](#)] [[PubMed](#)]
2. Xiong, Y.; Mahmood, A.; Chopp, M. Current understanding of neuroinflammation after traumatic brain injury and cell-based therapeutic opportunities. *Chin. J. Traumatol.* **2018**, *21*, 137–151. [[CrossRef](#)] [[PubMed](#)]
3. Ravula, A.R.; Teegala, S.B.; Kalakotla, S.; Pasangulapati, J.P.; Perumal, V.; Boyina, H.K. Fisetin, potential flavonoid with multifarious targets for treating neurological disorders: An updated review. *Eur. J. Pharmacol.* **2021**, *910*, 174492. [[CrossRef](#)] [[PubMed](#)]
4. Abdul-Muneer, P.M.; Schuetz, H.; Wang, F.; Skotak, M.; Jones, J.; Gorantla, S.; Zimmerman, M.C.; Chandra, N.; Haorah, J. Induction of oxidative and nitrosative damage leads to cerebrovascular inflammation in an animal model of mild traumatic brain injury induced by primary blast. *Free radical bio. Med.* **2013**, *60*, 282–291. [[CrossRef](#)] [[PubMed](#)]
5. Wang, Q.; Smith, R.E.; Luchtefeld, R.; Sun, A.Y.; Simonyi, A.; Luo, R.; Sun, G.Y. Bioavailability of apocynin through its conversion to glycoconjugate but not to diapocynin. *Phytomedicine* **2008**, *15*, 496–503. [[CrossRef](#)]
6. Chandasana, H.; Chhonker, Y.S.; Bala, V.; Prasad, Y.D.; Chaitanya, T.K.; Sharma, V.L.; Bhatta, R.S. Pharmacokinetic, bioavailability, metabolism and plasma protein binding evaluation of NADPH-oxidase inhibitor apocynin using LC-MS/MS. *J. Chromatogr. B Analyt. Technol. Biomed. Life Sci.* **2015**, *985*, 180–188. [[CrossRef](#)]
7. Lee, S.H.; Choi, B.Y.; Kho, A.R.; Jeong, J.H.; Hong, D.K.; Kang, D.H.; Kang, B.S.; Song, H.K.; Choi, H.C.; Suh, S.W. Inhibition of NADPH Oxidase Activation by Apocynin Rescues Seizure-Induced Reduction of Adult Hippocampal Neurogenesis. *Int. J. Mol. Sci.* **2018**, *19*, 3087. [[CrossRef](#)]
8. Ekozin, A.; Otuechere, C.A.; Adewuyi, A. Apocynin loaded silver nanoparticles displays potent in vitro biological activities and mitigates pyrogallol-induced hepatotoxicity. *Chem. Biol. Interact.* **2022**, *365*, 110069. [[CrossRef](#)]
9. Depciuch, J.; Jakubczyk, P.; Paja, W.; Sarzyński, J.; Pancierz, K.; Açikel Elmas, M.; Keskinöz, E.; Bingöl Özakpınar, Ö.; Arbak, S.; Özgün, G.; et al. Apocynin reduces cytotoxic effects of monosodium glutamate in the brain: A spectroscopic, oxidative load, and machine learning study. *Spectrochimica. Acta A.* **2022**, *279*, 121495. [[CrossRef](#)]
10. Kahles, T.; Luedike, P.; Endres, M.; Galla, H.J.; Steinmetz, H.; Busse, R.; Neumann-Haefelin, T.; Brandes, R.P. NADPH oxidase plays a central role in blood-brain barrier damage in experimental stroke. *Stroke* **2007**, *38*, 3000–3006. [[CrossRef](#)]
11. Singh, M.; Agarwal, S.; Tiwari, R.K.; Chanda, S.; Singh, K.; Agarwal, P.; Kashyap, A.; Panchar, P.; Mall, S.; R, R.; et al. Neuroprotective Ability of Apocynin Loaded Nanoparticles (APO-NPs) as NADPH Oxidase (NOX)-Mediated ROS Modulator for Hydrogen Peroxide-Induced Oxidative Neuronal Injuries. *Molecules* **2021**, *26*, 5011. [[CrossRef](#)] [[PubMed](#)]
12. Michaelis, K.; Hoffmann, M.M.; Dreis, S.; Herbert, E.; Alyautdin, R.N.; Michaelis, M.; Kreuter, J.; Langer, K. Covalent linkage of apolipoprotein e to albumin nanoparticles strongly enhances drug transport into the brain. *J. Pharmacol. Exp. Ther.* **2006**, *317*, 1246–1253. [[CrossRef](#)] [[PubMed](#)]
13. Brenza, T.M.; Ghaisas, S.; Ramirez, J.E.V.; Harischandra, D.; Anantharam, V.; Kalyanaraman, B.; Kanthasamy, A.G.; Narasimhan, B. Neuronal protection against oxidative insult by polyanhydride nanoparticle-based mitochondria-targeted antioxidant therapy. *Nanomedicine* **2017**, *13*, 809–820. [[CrossRef](#)] [[PubMed](#)]
14. Brenza, T.M.; Schlichtmann, B.W.; Bhargavan, B.; Vela Ramirez, J.E.; Nelson, R.D.; Panthani, M.G.; McMillan, J.M.; Kalyanaraman, B.; Gendelman, H.E.; Anantharam, V.; et al. Biodegradable polyanhydride-based nanomedicines for blood to brain drug delivery. *J. Biomed. Mater. Res. A* **2018**, *106*, 2881–2890. [[CrossRef](#)] [[PubMed](#)]
15. Aman, R.M.; Abu, H., II; Meshali, M.M. Novel chitosan-based solid-lipid nanoparticles to enhance the bio-residence of the miraculous phytochemical “Apocynin”. *Eur. J. Pharm. Sci.* **2018**, *124*, 304–318. [[CrossRef](#)]
16. Tang, X.N.; Cairns, B.; Cairns, N.; Yenari, M.A. Apocynin improves outcome in experimental stroke with a narrow dose range. *Neuroscience* **2008**, *154*, 556–562. [[CrossRef](#)] [[PubMed](#)]
17. Zensi, A.; Begley, D.; Pontikis, C.; Legros, C.; Mihoreanu, L.; Wagner, S.; Büchel, C.; von Briesen, H.; Kreuter, J. Albumin nanoparticles targeted with Apo E enter the CNS by transcytosis and are delivered to neurones. *J. Control. Release* **2009**, *137*, 78–86. [[CrossRef](#)]
18. Kuo, Y.C.; Lin, P.I.; Wang, C.C. Targeting nevirapine delivery across human brain microvascular endothelial cells using transferrin-grafted poly(lactide-co-glycolide) nanoparticles. *Nanomedicine (Lond)* **2011**, *6*, 1011–1026. [[CrossRef](#)]

19. Ding, S.; Khan, A.I.; Cai, X.; Song, Y.; Lyu, Z.; Du, D.; Dutta, P.; Lin, Y. Overcoming blood–brain barrier transport: Advances in nanoparticle-based drug delivery strategies. *Mater. Today* **2020**, *37*, 112–125. [[CrossRef](#)]
20. Saravanan, M.; Mostafavi, E.; Vincent, S.; Negash, H.; Andavar, R.; Perumal, V.; Chandra, N.; Narayanasamy, S.; Kalimuthu, K.; Barabadi, H. Nanotechnology-based approaches for emerging and re-emerging viruses: Special emphasis on COVID-19. *Microb. Pathog.* **2021**, *156*, 104908. [[CrossRef](#)]
21. Lu, C.T.; Zhao, Y.Z.; Wong, H.L.; Cai, J.; Peng, L.; Tian, X.Q. Current approaches to enhance CNS delivery of drugs across the brain barriers. *Int. J. Nanomed.* **2014**, *9*, 2241–2257. [[CrossRef](#)]
22. Siegal, T. Which drug or drug delivery system can change clinical practice for brain tumor therapy? *Neuro-oncology* **2013**, *15*, 656–669. [[CrossRef](#)] [[PubMed](#)]
23. An, F.F.; Zhang, X.H. Strategies for Preparing Albumin-based Nanoparticles for Multifunctional Bioimaging and Drug Delivery. *Theranostics* **2017**, *7*, 3667–3689. [[CrossRef](#)] [[PubMed](#)]
24. Ulbrich, K.; Hekmatara, T.; Herbert, E.; Kreuter, J. Transferrin- and transferrin-receptor-antibody-modified nanoparticles enable drug delivery across the blood-brain barrier (BBB). *Eur. J. Pharm. Biopharm.* **2009**, *71*, 251–256. [[CrossRef](#)] [[PubMed](#)]
25. Li, J.M.; Chen, W.; Wang, H.; Jin, C.; Yu, X.J.; Lu, W.Y.; Cui, L.; Fu, D.L.; Ni, Q.X.; Hou, H.M. Preparation of albumin nanospheres loaded with gemcitabine and their cytotoxicity against BXP-3 cells in vitro. *Acta Pharmacol. Sin.* **2009**, *30*, 1337–1343. [[CrossRef](#)] [[PubMed](#)]
26. Li, J.; Di, Y.; Jin, C.; Fu, D.; Yang, F.; Jiang, Y.; Yao, L.; Hao, S.; Wang, X.; Subedi, S.; et al. Gemcitabine-loaded albumin nanospheres (GEM-ANPs) inhibit PANC-1 cells in vitro and in vivo. *Nanoscale Res. Lett.* **2013**, *8*, 176. [[CrossRef](#)] [[PubMed](#)]
27. Yadav, K.S.; Sawant, K.K. Modified nanoprecipitation method for preparation of cytarabine-loaded PLGA nanoparticles. *AAPS Pharm. Sci. Tech.* **2010**, *11*, 1456–1465. [[CrossRef](#)]
28. Perumal, V.; Banerjee, S.; Das, S.; Sen, R.K.; Mandal, M. Effect of liposomal celecoxib on proliferation of colon cancer cell and inhibition of DMBA-induced tumor in rat model. *Cancer Nanotechnol.* **2011**, *2*, 67–79. [[CrossRef](#)]
29. Lee, M.S.; Kim, Y.H.; Kim, Y.J.; Kwon, S.H.; Bang, J.K.; Lee, S.M.; Song, Y.S.; Hahm, D.H.; Shim, I.; Han, D.; et al. Pharmacokinetics and biodistribution of human serum albumin-TIMP-2 fusion protein using near-infrared optical imaging. *J. Pharm. Pharm. Sci.* **2011**, *14*, 368–377. [[CrossRef](#)]
30. Lian, B.; Wu, M.; Feng, Z.; Deng, Y.; Zhong, C.; Zhao, X. Folate-conjugated human serum albumin-encapsulated resveratrol nanoparticles: Preparation, characterization, bioavailability and targeting of liver tumors. *Artif. Cells Nanomed. Biotechnol.* **2019**, *47*, 154–165. [[CrossRef](#)]
31. Nguyen, P.K.; Gao, W.; Patel, S.D.; Siddiqui, Z.; Weiner, S.; Shimizu, E.; Sarkar, B.; Kumar, V.A. Self-Assembly of a Dentinogenic Peptide Hydrogel. *ACS Omega* **2018**, *3*, 5980–5987. [[CrossRef](#)] [[PubMed](#)]
32. Bronze-Uhle, E.S.; Costa, B.C.; Ximenes, V.F.; Lisboa-Filho, P.N. Synthetic nanoparticles of bovine serum albumin with entrapped salicylic acid. *Nanotechnol. Sci. Appl.* **2016**, *10*, 11–21. [[CrossRef](#)] [[PubMed](#)]
33. Zaman, R.U.; Mulla, N.S.; Braz Gomes, K.; D'Souza, C.; Murnane, K.S.; D'Souza, M.J. Nanoparticle formulations that allow for sustained delivery and brain targeting of the neuropeptide oxytocin. *Int. J. Pharm.* **2018**, *548*, 698–706. [[CrossRef](#)]
34. Venkatesan, P.; Puvvada, N.; Dash, R.; Prashanth Kumar, B.N.; Sarkar, D.; Azab, B.; Pathak, A.; Kundu, S.C.; Fisher, P.B.; Mandal, M. The potential of celecoxib-loaded hydroxyapatite-chitosan nanocomposite for the treatment of colon cancer. *Biomaterials* **2011**, *32*, 3794–3806. [[CrossRef](#)]
35. Agas, A.; Garcia, R.; Kalluru, J.; Leiser, B.; Haorah, J. Synergistic effects of alcohol and HIV TAT protein on macrophage migration and neurotoxicity. *J. Neuroimmunol.* **2022**, *368*, 577869. [[CrossRef](#)] [[PubMed](#)]
36. Garcia-Pupo, L.; Zaldo-Castro, A.; Exarchou, V.; Tacoronte-Morales, J.E.; Pieters, L.; Vanden Berghe, W.; Nuñez-Figueroa, Y.; Delgado-Hernández, R. In Vitro Neuroprotective and Anti-Inflammatory Activities of Natural and Semi-Synthetic Spirosteroid Analogues. *Molecules* **2016**, *21*, 992. [[CrossRef](#)] [[PubMed](#)]
37. Yang, C.; Shi, Z.; You, L.; Du, Y.; Ni, J.; Yan, D. Neuroprotective Effect of Catalpol via Anti-Oxidative, Anti-Inflammatory, and Anti-Apoptotic Mechanisms. *Front. Pharmacol.* **2020**, *11*. [[CrossRef](#)]
38. Islam, Y.; Khalid, A.; Pluchino, S.; Sivakumaran, M.; Teixidó, M.; Leach, A.; Fatokun, A.A.; Downing, J.; Coxon, C.; Ehtezazi, T. Development of Brain Targeting Peptide Based MMP-9 Inhibiting Nanoparticles for the Treatment of Brain Diseases with Elevated MMP-9 Activity. *J. Pharm. Sci.* **2020**, *109*, 3134–3144. [[CrossRef](#)]
39. Wu, P.; Zhao, H.; Gou, X.; Wu, X.; Zhang, S.; Deng, G.; Chen, Q. Targeted delivery of polypeptide nanoparticle for treatment of traumatic brain injury. *Int. J. Nanomed.* **2019**, *14*, 4059–4069. [[CrossRef](#)]
40. Wang, H.L.; Lai, T.W. Optimization of Evans blue quantitation in limited rat tissue samples. *Sci. Rep.* **2014**, *4*, 6588. [[CrossRef](#)]
41. Elewa, H.F.; Hilali, H.; Hess, D.C.; Machado, L.S.; Fagan, S.C. Minocycline for short-term neuroprotection. *Pharmacotherapy* **2006**, *26*, 515–521. [[CrossRef](#)] [[PubMed](#)]
42. Suk, J.S.; Xu, Q.; Kim, N.; Hanes, J.; Ensign, L.M. PEGylation as a strategy for improving nanoparticle-based drug and gene delivery. *Adv. Drug Deliver. Rev.* **2016**, *99*, 28–51. [[CrossRef](#)] [[PubMed](#)]
43. Kuriakose, M.; Rama Rao, K.V.; Younger, D.; Chandra, N. Temporal and Spatial Effects of Blast Overpressure on Blood-Brain Barrier Permeability in Traumatic Brain Injury. *Sci. Rep.* **2018**, *8*, 8681. [[CrossRef](#)] [[PubMed](#)]
44. Kuriakose, M.; Younger, D.; Ravula, A.R.; Alay, E.; Rama Rao, K.V.; Chandra, N. Synergistic Role of Oxidative Stress and Blood-Brain Barrier Permeability as Injury Mechanisms in the Acute Pathophysiology of Blast-induced Neurotrauma. *Sci. Rep.* **2019**, *9*, 7717. [[CrossRef](#)]

45. Perumal, V.; Ravula, A.R.; Shao, N.; Chandra, N. Effect of minocycline and its nano-formulation on central auditory system in blast-induced hearing loss rat model. *J. Otol.* **2022**. [[CrossRef](#)]
46. Ravula, A.R.; Rodriguez, J.; Younger, D.; Perumal, V.; Shao, N.; Rama Rao, K.V.; Pfister, B.; Chandra, N. Animal model of repeated low-level blast traumatic brain injury displays acute and chronic neurobehavioral and neuropathological changes. *Exp. Neurol.* **2022**, *349*, 113938. [[CrossRef](#)]
47. Baratta, J.L.; Ngo, A.; Lopez, B.; Kasabwalla, N.; Longmuir, K.J.; Robertson, R.T. Cellular organization of normal mouse liver: A histological, quantitative immunocytochemical, and fine structural analysis. *Histochem. Cell Biol.* **2009**, *131*, 713–726. [[CrossRef](#)]
48. Wang, Y.; Li, S.Y.; Shen, S.; Wang, J. Protecting neurons from cerebral ischemia/reperfusion injury via nanoparticle-mediated delivery of an siRNA to inhibit microglial neurotoxicity. *Biomaterials* **2018**, *161*, 95–105. [[CrossRef](#)]
49. Mishra, V.; Mahor, S.; Rawat, A.; Gupta, P.N.; Dubey, P.; Khatri, K.; Vyas, S.P. Targeted brain delivery of AZT via transferrin anchored pegylated albumin nanoparticles. *J. Drug Target.* **2006**, *14*, 45–53. [[CrossRef](#)]
50. Torchilin, V.P. Drug targeting. *Eur. J. Pharm. Sci.* **2000**, *11*, 81–91. [[CrossRef](#)]
51. Niknejad, H.; Mahmoudzadeh, R. Comparison of Different Crosslinking Methods for Preparation of Docetaxel-loaded Albumin Nanoparticles. *Iran. J. Pharm. Res.* **2015**, *14*, 385–394.
52. Lohcharoenkal, W.; Wang, L.; Chen, Y.C.; Rojanasakul, Y. Protein Nanoparticles as Drug Delivery Carriers for Cancer Therapy. *BioMed. Res. Int.* **2014**, *2014*, 12. [[CrossRef](#)]
53. Motevalli, S.M.; Eltahan, A.S.; Liu, L.; Magrini, A.; Rosato, N.; Guo, W.; Bottini, M.; Liang, X.-J. Co-encapsulation of curcumin and doxorubicin in albumin nanoparticles blocks the adaptive treatment tolerance of cancer cells. *Biophys. Rep.* **2019**, *5*, 19–30. [[CrossRef](#)]
54. Mahobia, S.; Bajpai, J.; Bajpai, A.K. An In-vitro Investigation of Swelling Controlled Delivery of Insulin from Egg Albumin Nanocarriers. *Iran. J. Pharm. Res.* **2016**, *15*, 695–711.
55. Nan, A.; Bai, X.; Son, S.J.; Lee, S.B.; Ghandehari, H. Cellular uptake and cytotoxicity of silica nanotubes. *Nano. Lett.* **2008**, *8*, 2150–2154. [[CrossRef](#)] [[PubMed](#)]
56. Li, F.; Li, J.; Wen, X.; Zhou, S.; Tong, X.; Su, P.; Li, H.; Shi, D. Anti-tumor activity of paclitaxel-loaded chitosan nanoparticles: An in vitro study. *Mater. Sci. Eng.* **2009**, *29*, 2392–2397. [[CrossRef](#)]
57. Katanasaka, Y.; Ida, T.; Asai, T.; Shimizu, K.; Koizumi, F.; Maeda, N.; Baba, K.; Oku, N. Antiangiogenic cancer therapy using tumor vasculature-targeted liposomes encapsulating 3-(3,5-dimethyl-1H-pyrrol-2-ylmethylene)-1,3-dihydro-indol-2-one, SU5416. *Cancer Lett.* **2008**, *270*, 260–268. [[CrossRef](#)]
58. Juliana, K.d.O.; Debora, F.V.R.; Jociani, A.; Rubiana, M.M.; Najeh, M.K. Nanoencapsulation of Apocynin in Bovine Serum Albumin Nanoparticles: Physicochemical Characterization. *Nanosci. Nanotechnol.* **2018**, *8*, 90–99. [[CrossRef](#)]
59. Matos, A.C.; Pinto, R.V.; Bettencourt, A.F. Easy-Assessment of Levofloxacin and Minocycline in Relevant Biomimetic Media by HPLC-UV Analysis. *J. Chromatogr. Sci.* **2017**, *55*, 757–765. [[CrossRef](#)]
60. Ranjan, A.; Maples, D.; Newhardt, R.; Perumal, V. - Development of novel echogenic-imageable thermosensitive liposome for optimizing. *J. Ther. Ultrasound* **2015**, *3*, 73. [[CrossRef](#)]
61. Zhang, W.W.; Xu, F.; Wang, D.; Ye, J.; Cai, S.Q. Buyang Huanwu Decoction ameliorates ischemic stroke by modulating multiple targets with multiple components: In vitro evidences. *Chin. J. Nat. Med.* **2018**, *16*, 194–202. [[CrossRef](#)] [[PubMed](#)]
62. Heggannavar, G.B.; Vijeth, S.; Kariduraganavar, M.Y. Preparation of transferrin-conjugated poly- ϵ -caprolactone nanoparticles and delivery of paclitaxel to treat glioblastoma across blood–brain barrier. *Emergent Mater.* **2019**, *2*, 463–474. [[CrossRef](#)]
63. You, L.; Wang, J.; Liu, T.; Zhang, Y.; Han, X.; Wang, T.; Guo, S.; Dong, T.; Xu, J.; Anderson, G.J.; et al. Targeted Brain Delivery of Rabies Virus Glycoprotein 29-Modified Deferoxamine-Loaded Nanoparticles Reverses Functional Deficits in Parkinsonian Mice. *ACS Nano.* **2018**, *12*, 4123–4139. [[CrossRef](#)] [[PubMed](#)]
64. Perumal, V.; Sivakumar, P.M.; Zarrabi, A.; Muthupandian, S.; Vijayaraghavalu, S.; Sahoo, K.; Das, A.; Das, S.; Payyappilly, S.S.; Das, S. Near infra-red polymeric nanoparticle based optical imaging in Cancer diagnosis. *J. Photochem. Photobiol. B Biol.* **2019**, *199*, 111630. [[CrossRef](#)]

Disclaimer/Publisher’s Note: The statements, opinions and data contained in all publications are solely those of the individual author(s) and contributor(s) and not of MDPI and/or the editor(s). MDPI and/or the editor(s) disclaim responsibility for any injury to people or property resulting from any ideas, methods, instructions or products referred to in the content.